Pervasive transcription-dependent chromatin remodeling influences the replication initiation program

Julien Soudet[1]*, Jatinder Kaur[1] and Françoise Stutz[1]*.

[1]Dept. of Cell Biology, University of Geneva, Switzerland.

*Correspondence: julien.soudet@unige.ch, francoise.stutz@unige.ch

Keywords (10 words): non-coding RNA, pervasive transcription, histone modifications, nucleosomes, replication timing, replication initiation, yeast

Main text number of characters (with spaces): 55'000

ABSTRACT (149 words)

In Eukaryotic organisms, replication initiation follows a temporal program. Among the parameters that regulate this program in *Saccharomyces cerevisiae*, chromatin structure has been at the center of attention without considering the contribution of transcription. Here, we revisit the replication initiation program in the light of pervasive transcription. We find that non-coding RNA transcription termination in the vicinity of replication origins or ARS (Autonomously Replicating Sequences) maximizes replication initiation by restricting transcriptional readthrough into ARS. Consistently, high natural nascent transcription correlates with low ARS efficiency and late replication timing. High readthrough transcription is also linked to chromatin features such as high levels of H3K36me3 and deacetylated nucleosomes. Moreover, forcing ARS readthrough transcription promotes these histone modifications. Finally, replication initiation defects induced by increased transcriptional readthrough are partially rescued in the absence of H3K36 methylation. Altogether, these observations indicate that natural pervasive transcription into ARS influences replication initiation through chromatin remodeling.

INTRODUCTION

DNA replication is one of the fundamental processes occurring in all living organisms and ensuring accurate duplication of the genome. Eukaryotic replication initiation takes place at several dispersed locations termed replication origins. Origins are defined by a specific chromatin structure consisting of a nucleosome-depleted region (NDR) and the binding of specific replication initiation factors. In *Saccharomyces cerevisiae*, replication origins or ARS (Autonomously Replicating Sequences) are specified by an 11bp T-rich ARS consensus sequence (ACS) (Nieduszynski et al., 2006; Stinchcomb et al., 1979). ARS also contain more degenerate A-rich B elements proposed to contribute to origin function by excluding nucleosomes (Bell, 1995; Eaton et al., 2010; Segal and Widom, 2009). Despite the occurrence of thousands of ACS in the genome, only 200-300 are efficient for the recruitment of the AAA+ ATPase Origin Recognition Complex (ORC) (Hawkins et al., 2013; McGuffee et al., 2013; Raghuraman et al., 2001). During the G1-phase, ORC in conjunction with Cdt1 and Cdc6 promotes the binding of the MCM2-7 double hexamer helicase complex giving rise to the pre-replication complex (pre-RC) (Deegan and Diffley, 2016). The resulting ORC/MCM2-7-bound ARS are said to be licensed for replication initiation and have the ability to initiate replication during the subsequent S-phase (Aparicio, 2013).

Replication follows a temporal program of activation during S-phase. ARS are defined by an activation timing based on the observation that some ARS replicate earlier than others (Hawkins et al., 2013; Raghuraman et al., 2001). Moreover, using DNA combing, it appears that the fraction of cells in a population initiating replication at a given ARS is variable, defining a firing efficiency probability for each ARS (Czajkowsky et al., 2008; Hawkins et al., 2013; McGuffee et al., 2013). Nevertheless, timing and efficiency are linked, as inefficient origins tend to fire late during S-phase or to be replicated passively through the use of a neighboring origin (Yang et al., 2010). These two interdependent measurements of timing and efficiency are usually used to describe the replication initiation properties of ARS.

In *S. cerevisiae*, many parameters affect ARS activity including limiting trans-acting factors, different chromosomal location and/or sub-nuclear localization (Yoshida et al., 2013). ARS activity also depends on the chromatin context and histone modifications. First, early origins have a wider NDR than late ARS and adjacent nucleosomes are more precisely positioned (Rodriguez et al., 2017; Soriano et al., 2014). Moreover, the strength of ORC recruitment correlates with ARS activity and is itself important for NDR establishment (Belsky et al., 2015; Eaton et al., 2010). Second, early ARS activation during S-phase depends on histone acetylation (Unnikrishnan et al., 2010; Vogelauer et al., 2002). Indeed, the Class I Histone Deacetylase (HDAC) Rpd3 delays initiation of a huge number of replication origins (Aparicio et al., 2004; Knott et al., 2009; Vogelauer et al., 2002) and narrows their nucleosome depleted regions (Soriano et al., 2014).

Numerous studies attempting to consider transcription as another parameter to define replication initiation led to conflicting results. On one hand, transcription revealed some positive links with replication initiation, as highly transcribed genes were proposed to replicate earlier than low expressed genes (Fraser, 2013). Furthermore, stalled RNA polymerase II (RNAPII) was involved in the recruitment of ORC complex at the rDNA locus, and the activity of many replication origins depends on the presence of specific transcription factor binding sites (Knott et al., 2012; Mayan, 2013). On the other hand, active ARS are excluded from annotated ORFs and tend to localize after 3'-transcription terminators suggesting that transcription and replication initiation do not coexist (Nieduszynski et al., 2006). Furthermore, natural or artificial induction of transcription through origins leads to replication defects *via* dissociation or sliding of the pre-RC complex and MCMs respectively (Blitzblau et al., 2012; Gros et al., 2015; Mori and Shirahige, 2007b; Nieduszynski et al., 2005; Snyder et al., 1988). In this study, we aimed at clarifying the role of transcription in replication initiation in the context of pervasive transcription.

The analysis of appropriate mutants and the development of new tools to examine nascent transcription have revealed that the RNAPII transcriptional landscape in eukaryotic genomes extends far beyond mRNAs and stable non-coding RNAs (Churchman and Weissman, 2011; Schaughency et al., 2014). While 85% of the *S. cerevisiae* genome is transcribed, only 22% is devoted to protein-

coding genes (David et al., 2006). One source of pervasive transcription stems from widespread initiation at NDRs, an event controlled through early termination by the Nrd1-Nab3-Sen1 (NNS) complex recruited at the 5' end of all RNAPII transcription units through interaction with RNAPII C-terminal domain (CTD) (Arigo et al., 2006; Steinmetz et al., 2001). Recognition by Nrd1/Nab3 of specific motifs on the nascent RNA induces RNAPII termination usually within the first kilobase of transcription in a process coupled to degradation by the nuclear exosome component Rrp6 (Tudek et al., 2014). These cryptic unstable transcripts (CUTs) are revealed in the absence of Rrp6 (Jensen et al., 2013; Neil et al., 2009; van Dijk et al., 2011; Wyers et al., 2005; Xu et al., 2009). Similarly, depletion of Nrd1 results in transcriptional readthrough and accumulation of Nrd1 unterminated transcripts (NUTs), most of which correspond to extended CUTs (Schaughency et al., 2014; Schulz et al., 2013). Another source of pervasive transcription is linked to mRNA 3' end formation. The cleavage and polyadenylation (CPF) and cleavage factor (CF) complexes cleave the nascent mRNA just upstream of RNAPII. RNAPII release depends on a CPF-induced allosteric modification of the elongation complex as well as on the digestion of the generated 3' fragment by the 5'-3' exonuclease Rat1 (for a recent review see (Porrua et al., 2016). Thus, before being caught up by the so-called "torpedo", RNAPII continues transcription leading to an average 160bp-termination window after the polyadenylation site. Inefficient cleavage and polyadenylation can increase the level of this natural source of pervasive transcription (Baejen et al., 2017; Kim et al., 2004; Luo et al., 2006).

Using nascent transcription and replication analyses in strains depleted for early termination activities, we delineate how pervasive transcription negatively influences replication initiation by remodeling the chromatin structure of ARS. Our study clearly defines pervasive transcription as a new parameter regulating replication initiation.

RESULTS

CUTs and NUTs are enriched at early and efficient ARS

To determine the overlap of NUTs and CUTs with replication origins, we defined a list of 266 ARS (Suppl. Table 1) with previously annotated ACS (Nieduszynski et al., 2006; Soriano et al., 2014) and for which replication timing and efficiency had been established (Hawkins et al., 2013). Among the 266 well-defined ARS used in this analysis, 57 (21.5%) overlap with a CUT, a NUT or both (Figure 1A, Suppl. Figure 1A) (Schulz et al., 2013; Xu et al., 2009). The presence of CUTs and NUTs over 57 replication origins indicates that termination of non-coding transcription is particularly robust around these ARS. Notably, the 57 ARS enriched with NUTs and/or CUTs (ncARS) are replicated earlier and more efficiently than the remaining 209 ARS (Other ARS) (Figure 1B). These observations suggest that non-coding transcription termination may be an important determinant of ARS replication timing and efficiency.

Non-coding transcription readthrough affects replication initiation

To investigate the effect of non-coding transcription readthrough on replication, early termination of non-coding RNAs was abrogated by rapid nuclear depletion of Nrd1 through anchor away (AA) (Haruki et al., 2008). Nrd1 depletion, induced by addition of Rapamycin (Rap) to the engineered Nrd1-AA strain, is accompanied by transcription elongation and accumulation of NUTs (Schulz et al., 2013). To examine the effect on replication, the Nrd1-AA strain was treated with alpha factor to synchronize the cells in G1-phase and incubated an additional hour -/+ Rap to induce non-coding transcription. Cells were then released from G1 arrest in the presence of BrdU (Figure 1C). FACS analyses indicate a slight cell cycle delay at 80 min in cells depleted for Nrd1, with an increased number of cells in G1 in +Rap compared to –Rap (Suppl. Figure 1B). Samples were harvested for BrdU-seq at 70min after G1-phase release. Visualization of the data revealed a number of well-defined peaks centered on specific ARS (Figure 1D, Suppl. Figure 1C and 1D). Global analysis of the BrdU-seq showed that out of the 193 selected early ARS, 39 (20.2%) present a

reproducible, more than 35% decrease in BrdU incorporation in + Rap versus – Rap (18 show >50% decrease and 21 between 35-50% decrease) (Figure 1E). Consistently, metagene analysis from -10Kb to +10Kb around the ACS of the >50% affected ARS revealed a substantial reduction in the BrdU-seq profile in the presence of Rap, while the curves including the <35% affected ARS presented only a slight change in +Rap versus -Rap (Figure 1F). Affected ARS showed a nice overlap with the NUTs-containing ARS defined in Figure 1A (Suppl. Figure 1E). To define whether the decreased BrdU-seq signal of affected ARS upon Nrd1 depletion was linked to transcription, RNAPII PAR-CLIP data from the Corden lab (Schaughency et al., 2014) were used to examine the level of nascent transcription over ARS when depleting Nrd1. Strikingly, the ARS with the strongest decrease in BrdU incorporation in +Rap versus –Rap also showed the highest increase in nascent RNAPII transcription (Figures 1D and G). Thus, the replication defect observed following Nrd1 depletion is directly linked to increased nascent transcription through the affected ARS.

RNA and BrdU analyses were also performed with the Rrp6-AA strain. Depletion of Rrp6 resulted in similar effects on ncRNA accumulation and replication initiation (Suppl. Figure 2).

Overall, these data suggest that replication initiation may be hindered by non-coding readthrough transcription.

High non-coding readthrough transcription leads to ARS chromatin remodeling

Given the links between replication initiation and chromatin structure, we then analyzed the effects of the Nrd1 depletion-induced transcription readthrough into replication origins on nucleosome positioning. To do so, chromatin was extracted from Nrd1-AA cells either untreated or treated for 1 hour with Rapamycin and digested with micrococcal nuclease (MNase). First, sequencing of the fragments protected by nucleosomes revealed the typical NDR around the ACS as previously described (Figure 2A) (Eaton et al., 2010). Second, analysis of nucleosome positioning at the classes of ARS defined in Figure 1E, revealed a statistically significant increased occupancy in the NDRs of the ARS

that are the most affected for replication initiation and present a higher increase in readthrough transcription (Figures 2A, B and C and Figure 1G). This result suggests that high levels of pervasive transcription into replication origins leads to chromatin remodeling which may in turn perturb replication initiation. Additional parameters are likely to influence replication since the mildly affected ARS (35-50%) do not show chromatin remodeling although they are affected in replication initiation.

ARS with high basal level of readthrough transcription are late and inefficient

Recent data show that non-coding transcription occurs all over eukaryotic genomes (Jensen et al., 2013) and our results indicate that non-coding transcription is detrimental for replication initiation. These observations led to the hypothesis that differences in nascent transcription between ARS may influence both their activity and chromatin structure at steady-state. First, we confirmed that the production of stable transcripts, defined by RNA-seq, strongly drops in the vicinity of the 266 replication origins (including both early and late origins), while profiles of nascent transcription indicate that RNA PolII density stays relatively constant through these ARS (Figures 3A and B). These observations clearly establish that non-coding transcription through replication origins is a frequent event. The set of ARS was then analysed for the level of natural basal readthrough transcription over a 100bp segment between the ACS and the B elements using published RNA PolII PAR-CLIP data (Schaughency et al., 2014). This analysis identified a group of 43 ARS with a median value of nascent transcription 5 fold higher compared to the second group of 223 ARS with lower natural readthrough transcription (Figure 3C). The highly transcribed ARS were significantly enriched in ARS lying between two convergent genes (Suppl. Figure 3A). Importantly, nascent transcription towards the ARS measured from upstream and downstream of the oriented ACS were also significantly different for the two groups (Suppl. Figure 3B), indicating that high ARS readthrough mainly stems from higher levels of nascent transcription from the adjacent convergent genes. Interestingly, running these two groups of ARS through

replication timing and efficiency data (Hawkins et al., 2013) revealed that the 43 ARS with high readthrough transcription have a significantly delayed replication timing and reduced replication efficiency compared to the ARS with lower transcriptional readthrough (Figure 3D). Notably, the 57 NUTs/CUTs-containing ARS present significantly lower natural readthrough transcription than the highly transcribed ARS, further supporting that NNS-mediated termination positively contributes to replication timing and efficiency by shielding ARS form pervasive transcription (Suppl. Figure 3C). Consistent with these results, earlier defined ORC-bound ARS (ORC-ARS) exhibit significantly less readthrough transcription compared to non ORC-bound and non-replicated ARS (nr-ARS) (Suppl. Figure 3D) (Eaton et al., 2010).

Steady-state highly transcribed ARS present distinctive chromatin features

Using recently published nucleosome occupancy and histone modification data (Kubik et al., 2015; Weiner et al., 2015), the 43 ARS with high pervasive transcription appear to be associated with increased nucleosome occupancy compared to the 223 with lower transcription levels (Figure 3E); these 43 ARS also present higher levels of the H3K36me3 mark (Figure 3F) and lower levels of H3K18, H3K14, H4K12 and H4K5 acetylations (Figure 3G and Suppl. Figures 4A, B and C). Interestingly, H3K36me3 is deposited by the Set2 histone methyl transferase and leads to the recruitment of the Rpd3 HDAC known to deacetylate the lysines cited above and described as being involved in replication control (Knott et al., 2009; Rundlett et al., 1996). In contrast, the two groups of ARS present no difference in H3K4me2, another mark promoting deacetylation of the chromatin via binding of the Set3 HDAC (Supp. Figure 4D) (Woo et al., 2017).

Finally, using recently published ORC ChIP-seq data (Belsky et al., 2015), the group of 43 ARS also shows reduced ORC binding compared to the other 223 ARS (Figure 3H). Together these observations support the view that pervasive transcription through an ARS promotes the formation of a closed chromatin structure reducing its ability to interact with ORC, thereby decreasing its efficiency and/or delaying its replication timing.

mRNA and non-coding readthrough transcription over ARS induce H3K36 methylation, histone deacetylation and increased nucleosome occupancy.

To strengthen the causal relationship between nascent transcription, changes in chromatin organization and ARS activity, we examined the effect of induced transcription on ARS chromatin remodeling. Since 86% of replication origins are located in the vicinity of a convergent coding gene, we decided to anchor away the essential mRNA 3' cleavage and polyadenylation factor (CPF/CF) endonuclease Ysh1. As expected, anchoring away Ysh1 has a major impact on replication progression and more specifically on replication initiation, as most of the 193 considered ARS showed reduced BrdU incorporation in the presence of rapamycin, with 29 ARS presenting more than 80% decrease (Figures 4A and B, Suppl. Figures 5A and B). Combining BrdU-Seq in Ysh1-AA -/+ Rap with published RNA PolII PAR-CLIP data of this strain (Schaughency et al., 2014) revealed that the 29 ARS with the strongest replication defect also present the highest increase in readthrough transcription (Figure 4C and Suppl. Figure 5C). Furthermore, nascent RNA PolII transcription in -/+ Rap was examined at the 193 ARS subdivided into 4 classes based on their configuration (Figure 4D). ARS from each class were then ranked according to the total readthrough increase observed following Ysh1 depletion (Figure 4D). To relate the replication defect induced by mRNA readthrough transcription to changes in chromatin structure, chromatin immunoprecipitation was used to compare Histone H3 occupancy, H3K36 methylation and H3K18 acetylation in -/+ Rap at 3 highly affected ARS and 3 non-affected ARS as control (respectively labeled in red and green in Figure 4D). Primers for qPCR were designed to target the NDR of the ARS. At the 3 affected ARS, rapamycin treatment resulted in increased H3 occupancy (except for ARS507) and H3K36 methylation as well as a decrease in H3K18 acetylation, while no changes were observed at the non-affected ARS (Figures 4E, F and G). Moreover, consistent with the replication data, rapamycin treatment led to a strong decrease in ORC recruitment at the affected ARS but not at the control ARS (Figure 4H).

The same chromatin analyses were performed in the Nrd1-AA strain following induction of non-coding readthrough transcription and led to similar

observations, *i.e* H3 and H3K36me3 increased while H3K18ac decreased upon Nrd1 depletion at the ARS most affected in this strain (Suppl. Figures 6A, B, C and D).

Taken together, these experiments demonstrate that increased readthrough transcription causes increased nucleosome occupancy and histone deacetylation at the downstream ARS, two parameters described to interfere with the efficiency of ORC binding and ARS licensing (Aparicio et al., 2004; Knott et al., 2009; Soriano et al., 2014; Vogelauer et al., 2002).

Replication defects induced by non-coding readthrough transcription are partially rescued in the absence of H3K36 methylation

To decipher the molecular cascade of events, we analyzed the effects of non-coding transcription readthrough on replication initiation in a Nrd1-AA *set2Δ* strain (Figure 5A). Global analysis of replication by flow cytometry indicates that replication is still delayed in the absence of H3K36 methylation in the Nrd1-AA background (Suppl. Figure 7A). However, by taking the same classes of defective ARS as defined in Figure 1, we observed a partial rescue of BrdU incorporation (Figures 5B, C and D) although non-coding RNAs were still produced in the absence of Set2 (Suppl. Figure 7B). These observations support the view that pervasive transcription drives chromatin remodeling of replication origins, which in turn defines, at least in part, ARS activity.

Interestingly, rapamycin treatment of the Nrd1-AA *set2Δ* strain led to the appearance of small BrdU incorporation peaks all over the genome (Figure 5D), suggesting that replication initiation loses its specificity when both non-coding transcription termination and H3K36 methylation are abrogated. Moreover, analysis of BrdU incorporation around non-ORC bound and non-replicated ACS (Eaton et al., 2010) revealed an increase of replication initiation at non-canonical sites when non-coding transcription readthrough is induced in the absence of Set2 (Figures 5E and F). Thus, while non-coding transcription interferes with replication in the presence of Set2 by favoring a closed chromatin structure,

transcription over dormant ARS in the absence of Set2 activates replication, probably as a result of nucleosome instability.

DISCUSSION

We have shown that ncRNA early termination by the Nrd1-dependent pathway in the vicinity of a subset of ARS protects these origins from transcription and replication initiation defects. These observations suggest that inefficient non-coding transcription termination may influence replication origin activity. Consistently, our analyses reveal that natural readthrough transcription correlates with reduced ARS activity and a specific replication origin chromatin structure. Moreover, using mRNA or cryptic transcription termination mutants, we have established that nascent transcription is the causal link defining chromatin organization at a number of ARS. Finally, we have presented evidence that pervasive transcription-induced chromatin modifications and not only pervasive transcription *per se* controls ARS activity. Thus, we propose pervasive transcription as a novel primordial parameter defining replication initiation features (Figure 6).

Nrd1-dependent transcription termination protects a subset of early/efficient replication origins from pervasive transcription

Previous studies on the relationship between transcription and replication have led to conflicting observations. Our analyses of pervasive transcription lead to the conclusion that transcriptional readthrough at ARS is detrimental for replication initiation as already proposed by some reports (Blitzblau et al., 2012; Gros et al., 2015; Mori and Shirahige, 2007a; Snyder et al., 1988). Importantly, however, we show that natural nascent transcription *per se* is a criterion defining ARS activity genome-wide. Thus, the strategy for a replication origin to increase its activity would be to limit pervasive transcription. Accordingly, a subset of early and efficient ARS are protected from pervasive transcription thanks to surrounding non-coding transcription termination by the Nrd1-dependent pathway (Figures 1, 3 and Supp. Figure 3C). Thus, we propose that Nrd1-dependent termination in the vicinity of a replication origin is an efficient way to decrease transcriptional readthrough. Since Nrd1-dependent termination is regulated under stress conditions, it is tempting to speculate that this might also impact on replication origins usage

(Bresson et al., 2017; van Nues et al., 2017). This scenario would define a novel role for non-coding RNAs in the regulation of genome maintenance.

Interestingly, no mechanism similar to Nrd1-dependent termination has been described in other eukaryotes yet (Wittmann et al., 2017). In *S. cerevisiae*, Nrd1-protected origins reach a median firing efficiency peaking at 58%, while firing efficiency is around 30% in *Schizosaccharomyces pombe* (Heichinger et al., 2006). An attractive view is that Nrd1-dependent transcription termination represents an evolutionary pathway maximizing replication initiation efficiency.

Importantly, there is no significant linear correlation between nascent transcription and ARS activity. This connection appears when ARS are divided into subsets (Figure 3). These observations indicate that nascent transcription influences ARS activity only beyond a certain threshold and that other parameters contribute to origin function. Accordingly, a variety of molecular events have been involved in regulating ARS activity, which include MCM levels bound to ARS, cell cycle regulated binding and affinity of the ORC complex for the ACS, or the presence of Fkh1/2 proteins (Belsky et al., 2015; Das et al., 2015; Hoggard et al., 2013; Looke et al., 2013; Peace et al., 2016).

Replication origin chromatin structure is influenced by pervasive readthrough transcription

Previous work has involved the chromatin structure at replication origins as a parameter defining replication initiation. Early ARS tend to show an open chromatin, low H3K36me3 and high histone acetylation levels (Pryde et al., 2009; Soriano et al., 2014). Our results indicate that these features may be directly related to the level of natural nascent transcription. Indeed, when compared to highly transcribed ARS, origins with low level of readthrough transcription are characterized by lower nucleosome occupancy, lower H3K36me3 and higher histone acetylation levels (Figure 3). Notably, H3K36me3 is deposited by Set2, a histone methyl transferase (HMT) recruited through interaction with the C-terminal domain (CTD) of the elongating RNAPII. H3K36me3 serves as a platform for the binding of Rpd3S, a histone deacetylase complex described to deacetylate and stabilize reassembled nucleosomes in the

wake of the transcription machinery, suppressing initiation from cryptic sites within ORFs (Carrozza et al., 2005) and see (Woo et al., 2017) for a recent review. This molecular mechanism may represent the connection between pervasive transcription and chromatin structure of replication origins. Indeed, increasing transcriptional readthrough into replication origins is accompanied by higher levels of H3K36me3, lower levels of H3K18ac, increased nucleosome occupancy and replication defects (Figures 2 and 4, and Suppl. Figure 6). Importantly, BrdU-seq experiments cannot discriminate between timing and efficiency defects. However, since nucleosome methylations are relatively stable modifications, it would be appealing to propose that even rare events of pervasive transcription may stably inactivate replication origins until the subsequent S-phase dilutes or a histone demethylase erases these methylation marks In such a model, pervasive transcription may shape replication origin chromatin for inefficient usage.

These observations shed new light on earlier published results. First, loss of Rpd3 leads to a global increase in acetylation around ARS and early firing of many late origins (Knott et al., 2009; Vogelauer et al., 2002). It was proposed that the "accelerated" replication in *rpd3Δ* is mainly due to a reduced titration of replication initiation factors by the rDNA origins (Yoshida et al., 2014); however, loss of Rpd3 also has a global impact on increasing the size of replication origins NDR (Soriano et al., 2014). Of note, loss of Rpd3 abrogates the function of both Rpd3S and Rpd3L, another histone deacetylase complex involved in gene repression following recruitment to promoters via a Set2/H3K36met3 independent pathway (Woo et al., 2017). While loss of Rpd3L subunits was shown to result in increased BrdU incorporation at a number of ARS, especially those adjacent to upregulated genes, loss of Rpd3S subunits or Set2 led to a weaker but more generalized increase in ARS replication initiation (Knott et al., 2009). This difference could reflect a primary specific effect of loss of Rpd3L on rDNA replication and increased availability of replication factors in the absence of this HDAC. Although the replication phenotype was less pronounced when deleting Rpd3S, the data support the view that pervasive transcription promotes Set2/H3K36me3-mediated histone deacetylation by Rpd3S and globally contributes to negatively regulate replication origin activity.

Our results further indicate that high readthrough transcription correlates with decreased ORC binding (Figure 3 and Suppl. Fig. 3D). It was proposed that replication initiation timing depends more on the surrounding chromatin than on the ORC-ACS *in vitro* affinity by itself (Hoggard et al., 2013). It would be interesting to further dissect the molecular events at origins and to define whether nascent transcription *per se* evicts ORC complex, leading to nucleosome deposition and histone modifications, or whether RNAPII readthrough and nucleosome incorporation outcompete ORC turnover (Figure 6).

Surprisingly, we observe genome-wide appearance of BrdU peaks when *SET2* is deleted in conjunction with the anchor-away of Nrd1. These peaks are not detected in the *set2Δ* mutant alone indicating that activation of dormant origins is not only related to the absence of the histone mark. Deletion of *SET2* is known to drastically increase the level of intragenic transcription initiation (Malabat et al., 2015). A fraction of this novel nascent transcription may be cleared by the Nrd1-dependent termination pathway. We propose that in the absence of Nrd1, transcription may hit dormant origins, which in the absence of H3K36 methylation will promote replication initiation due to nucleosome instability and chromatin opening. Thus, when not associated with H3K36 methylation, transcription may have a positive effect on replication initiation.

Implications for a pervasive transcription-dependent replication initiation model in metazoans

Identification of replication origins in mouse embryonic stem cells showed that nearly half of them are contained in promoters (Sequeira-Mendes et al., 2009), and recent ORC binding data in human cells led to the same conclusion (Dellino et al., 2013; Miotto et al., 2016). In contrast, replication initiation in *S. cerevisiae* more frequently occurs next to gene terminators (Nieduszynski et al., 2006). Interestingly, human promoters are bidirectional and lead to the production of highly unstable promoter upstream transcripts (PROMPTs), suggesting that pervasive transcription could also play a role in metazoan replication initiation (Mayer et al., 2015; Nojima et al., 2015; Preker et al., 2008).

It has recently been shown that replication initiation in human cells occurs within broad over 30kb regions, flanked by ORC binding at one of the two ends (Petryk et al., 2016). Considering that MCM helicases can slide along the chromosome with the help of transcription (Gros et al., 2015), it would be appealing to propose that promoter-associated pervasive transcription redistributes the MCM helicases from their ORC binding initial site of loading. Since we have established pervasive transcription as a novel primordial parameter regulating replication initiation in *S. cerevisiae*, its importance for the metazoan replication program will deserve being studied in the next few years.

EXPERIMENTAL PROCEDURES

Yeast strains and Microbiological methods

All strains were derived from W303 and Anchor-Away genetic backgrounds (see Supplementary Table 2) (Haruki et al., 2008). Cells were grown in YEPD medium (1% yeast extract, 1% peptone) supplemented with 2% glucose as the carbon source**.** The BrdU incorporation cassette was introduced according to (Viggiani and Aparicio, 2006). Anchor-away of Nrd1-AA*,* Nrd1-AA *set2Δ,* Rrp6-AA or Ysh1-AA strains was induced by adding 1µg/ml of rapamycin to the medium.

Cell culture and FACS analyses

Cells grown at 30°C to an OD600= 0.4 were synchronized in G1-phase with α-factor (20 ng/ml, Sigma) for 3h in total. After two washes with distilled water, cells were released into S-phase at 18°C. Depending on the experiment, cells were released in YEPD medium containing BrdU (100 µg/ml, Sigma) and treated or not with rapamycin. Cells were then collected at different times after G1-release depending on the experiment and treated with 0.1% Sodium Azide (Sigma). Flow cytometry was performed on ethanol-fixed cells using propidium iodide (Sigma). Flow cytometry profiles were obtained using Gallios flow cytometer (Beckman-Coulter) before data analyses using FlowJo software (LLC).

RNA extraction and Reverse Transcription-qPCR

RNAs were extracted using Trizol (Invitrogen). Purified nucleic acids were first treated with DNAse (Ambion) before reverse transcription using SuperScript II (Invitrogen). cDNA was then amplified as described below using the primers available upon request.

BrdU immunoprecipitation and sequencing

BrdU immunoprecipitation was mainly performed as described in (Soudet et al., 2014) with the following modifications. Genomic DNA was sonicated into 300-400 bp fragments and denatured. 5µg BrdU antibody (BD PharMingen, 555627)

coupled to 75µl of Dynabeads Protein G (Invitrogen) were added to 5µg of denatured BrdU-containing genomic DNA in BrdU IP buffer (PBS + 0.0625% Triton X-100). After 1 hour incubation at room temperature on a wheel, beads were washed twice with BrdU IP buffer and eluted in Tris-HCl 10mM (pH 8.0), EDTA 1mM, 1% SDS. Eluates were cleared of SDS using the NucleoSpin Gel and PCR Clean-up (Macherey-Nagel). Libraries were constructed using the iDeal library preparation kit (Diagenode). Sequencing was performed on the HiSeq 4000 sequencer (Illumina). For specific loci analyses by quantitative PCR, BrdU-containing DNA was amplified using the SYBR select master mix for CFX (Applied Biosciences) on a CFX96 Real-time detection system (Bio-Rad).

Mnase-seq

MNase treatment was performed as described in (Weiner et al., 2015). Chromatin was extracted by breaking cells with bead beating in a magnalyser (Roche). Chromatin was then collected by centrifugation and re-suspended in NP-buffer (0.5 mM spermidine, 1 mM β-ME, 0.075% NP40, 50 mM NaCl, 10 mM Tris pH 7.4, 5 mM MgCl2, 1 mM CaCl2). MNase (Thermo-Scientific) treatment was performed at a previously optimized concentration to have comparable intensity of both mono- and di-nucleosomes within and between the samples. MNase treatment was followed by de-crosslinking, protease treatment and DNA was extracted using NucleoSpin gel and PCR extraction columns (Macherey-Nagel). iDeal library preparation kit (Diagenode) was then used for library construction. Sequencing was performed on the HiSeq 4000 sequencer (Illumina).

BrdU-seq and MNase-seq bioinformatic analyses

50bp paired-end reads were aligned to sacCer3 genome assembly using HTSstation (David et al., 2014). PCR duplicates were removed from the analysis. BrdU-seq density files (bigwig) were averaged for the two replicates of each condition. All subsequent analyses were performed using HTS Bioscript (David et al., 2014). To assign one value of BrdU incorporation to each ARS, BrdU incorporation was measured 5kb around ACSs considering this area as 1bin.

Since no spike-in was used in our experiments and since Nrd1-AA *set2Δ* + Rap substantially changes the density profile because of dormant origins firing, Figure 5 was normalized as follows: the <35% affected ARS class for BrdU incorporation was considered as equal in +Rap and -Rap in average 5kb around the ACS in both Nrd1-AA and Nrd1-AA *set2Δ*. This gave a normalization factor for each strain, which was then used to quantify the other classes.

Transcriptional readthrough calculation for RNAPII PAR-CLIP

Induced transcriptional readthrough was calculated as follows. First, mean densities of Watson and Crick strands in each condition were calculated on oriented ARS between the ACS to +100bp considering this region as 1bin. A pseudo-count of 1 was added to each value to correct for low values, which could lead to overestimated ratios defined hereafter. The total readthrough was then calculated by adding the values obtained for Watson and Crick in +Rap divided by the sum of Watson and Crick in –Rap.

Chromatin Immunoprecipitation (ChIP)

ChIP experiments were performed as described previously with some modifications (Camblong et al., 2007). Antibodies against H3 (Abcam ab1791), H3K36me3 (Abcam ab9050), H3K18ac (Abcam ab1191) and ORC (gift from S. Bell) were incubated with Protein G dynabeads (Invitrogen) before being mixed with sonicated chromatin and incubated on a wheel at 4°C for 2 hours. After washes, immunoprecipitated chromatin was eluted before being purified on columns (Macherey-Nagel). ChIPs were repeated three times with different chromatin extracts from independent cultures. Immunoprecipitated DNA was then purified and quantified by qPCR.

List of non-coding RNAs and replication origins

The list of CUTs was obtained from (Xu et al., 2009), while the list of NUTs was kindly provided by the Cramer lab (Schulz et al., 2013). Among the NUTs, only those showing at least a 2-fold increase in +Rap/-Rap were taken into account to unify the threshold of ncRNA definition between CUTs and NUTs. The list of ARS

(Supplementary Table 1) consists of the 266 ACS taken from (Soriano et al., 2014) that overlap with the replication origins described in (Hawkins et al., 2013), for which replication timing and efficiency have been defined.

Statistical analysis

All statistical analyses of this work were performed using Prism 7.0 (Graphpad). All tests are non-paired tests (with the exception of Figure 5C). T-tests or Mann-Whitney tests were used according to the normality of the data analyzed, which was calculated using a d'Agostino-Pearson omnibus normality test.
* for p-value<0.05; ** <0.01; ***<0.001 and ****<0.0001.

Bioinformatics data availability

The accession number for the raw and processed sequencing data reported in this paper is GEO: GSE111058.

Published datasets used for analyses

For RNA PolII PAR-CLIP, RNA-seq, chromatin and ORC profiles, data were retrieved from (Schaughency et al., 2014) (GEO: GSE56435), (Uwimana et al., 2017) (GEO: GSE89601), (Kubik et al., 2015) (GEO: GSE73337), (Weiner et al., 2015) (GEO: GSE61888) and (Belsky et al., 2015) (SRA: SRP041314).

Author Contributions

J.S. and F.S. conceived the study. J.S. performed most experiments and analyzed the results together with F.S.; J.K. performed the MNAse-seq; J.S. and F.S. wrote the manuscript.

AKNOWLEDGEMENTS

We would like to thank O. Aparicio, S. Bell, D. MacAlpine and P. Cramer for sharing data and reagents; M. Strubin, F. Steiner, M. Shyian, G. Canal, T. Halazonetis and all members from the Stutz lab for comments on the manuscript. We also would like to thank Domenico Libri for communication of unpublished results. This work was funded by the Swiss National Science Foundation (31003A 153331), iGE3 and the Canton of Geneva, as well as a Polish Swiss Research Programme (PSRP NoCore 183/2010).

REFERENCES

Aparicio, J.G., Viggiani, C.J., Gibson, D.G., and Aparicio, O.M. (2004). The Rpd3-Sin3 histone deacetylase regulates replication timing and enables intra-S origin control in Saccharomyces cerevisiae. Mol Cell Biol *24*, 4769-4780.

Aparicio, O.M. (2013). Location, location, location: it's all in the timing for replication origins. Genes & development *27*, 117-128.

Arigo, J.T., Eyler, D.E., Carroll, K.L., and Corden, J.L. (2006). Termination of cryptic unstable transcripts is directed by yeast RNA-binding proteins Nrd1 and Nab3. Molecular cell *23*, 841-851.

Baejen, C., Andreani, J., Torkler, P., Battaglia, S., Schwalb, B., Lidschreiber, M., Maier, K.C., Boltendahl, A., Rus, P., Esslinger, S.*, et al.* (2017). Genome-wide Analysis of RNA Polymerase II Termination at Protein-Coding Genes. Molecular cell.

Bell, S.P. (1995). Eukaryotic replicators and associated protein complexes. Current opinion in genetics & development *5*, 162-167.

Belsky, J.A., MacAlpine, H.K., Lubelsky, Y., Hartemink, A.J., and MacAlpine, D.M. (2015). Genome-wide chromatin footprinting reveals changes in replication origin architecture induced by pre-RC assembly. Genes & development *29*, 212-224.

Blitzblau, H.G., Chan, C.S., Hochwagen, A., and Bell, S.P. (2012). Separation of DNA replication from the assembly of break-competent meiotic chromosomes. PLoS genetics *8*, e1002643.

Bresson, S., Tuck, A., Staneva, D., and Tollervey, D. (2017). Nuclear RNA Decay Pathways Aid Rapid Remodeling of Gene Expression in Yeast. Molecular cell *65*, 787-800 e785.

Camblong, J., Iglesias, N., Fickentscher, C., Dieppois, G., and Stutz, F. (2007). Antisense RNA stabilization induces transcriptional gene silencing via histone deacetylation in S. cerevisiae. Cell *131*, 706-717.

Carrozza, M.J., Li, B., Florens, L., Suganuma, T., Swanson, S.K., Lee, K.K., Shia, W.J., Anderson, S., Yates, J., Washburn, M.P.*, et al.* (2005). Histone H3 methylation by Set2 directs deacetylation of coding regions by Rpd3S to suppress spurious intragenic transcription. Cell *123*, 581-592.

Churchman, L.S., and Weissman, J.S. (2011). Nascent transcript sequencing visualizes transcription at nucleotide resolution. Nature *469*, 368-373.

Czajkowsky, D.M., Liu, J., Hamlin, J.L., and Shao, Z. (2008). DNA combing reveals intrinsic temporal disorder in the replication of yeast chromosome VI. J Mol Biol *375*, 12-19.

Das, S.P., Borrman, T., Liu, V.W., Yang, S.C., Bechhoefer, J., and Rhind, N. (2015). Replication timing is regulated by the number of MCMs loaded at origins. Genome Res *25*, 1886-1892.

David, F.P., Delafontaine, J., Carat, S., Ross, F.J., Lefebvre, G., Jarosz, Y., Sinclair, L., Noordermeer, D., Rougemont, J., and Leleu, M. (2014). HTSstation: a web application and open-access libraries for high-throughput sequencing data analysis. PLoS One *9*, e85879.

David, L., Huber, W., Granovskaia, M., Toedling, J., Palm, C.J., Bofkin, L., Jones, T., Davis, R.W., and Steinmetz, L.M. (2006). A high-resolution map of transcription in the yeast genome. Proceedings of the National Academy of Sciences of the United States of America *103*, 5320-5325.

Deegan, T.D., and Diffley, J.F. (2016). MCM: one ring to rule them all. Current opinion in structural biology *37*, 145-151.

Dellino, G.I., Cittaro, D., Piccioni, R., Luzi, L., Banfi, S., Segalla, S., Cesaroni, M., Mendoza-Maldonado, R., Giacca, M., and Pelicci, P.G. (2013). Genome-wide mapping of human DNA-replication origins: levels of transcription at ORC1 sites regulate origin selection and replication timing. Genome Res *23*, 1-11.

Eaton, M.L., Galani, K., Kang, S., Bell, S.P., and MacAlpine, D.M. (2010). Conserved nucleosome positioning defines replication origins. Genes & development *24*, 748-753.

Fraser, H.B. (2013). Cell-cycle regulated transcription associates with DNA replication timing in yeast and human. Genome Biol *14*, R111.

Gros, J., Kumar, C., Lynch, G., Yadav, T., Whitehouse, I., and Remus, D. (2015). Post-licensing Specification of Eukaryotic Replication Origins by Facilitated Mcm2-7 Sliding along DNA. Molecular cell *60*, 797-807.

Haruki, H., Nishikawa, J., and Laemmli, U.K. (2008). The anchor-away technique: rapid, conditional establishment of yeast mutant phenotypes. Molecular cell *31*, 925-932.

Hawkins, M., Retkute, R., Muller, C.A., Saner, N., Tanaka, T.U., de Moura, A.P., and Nieduszynski, C.A. (2013). High-resolution replication profiles define the stochastic nature of genome replication initiation and termination. Cell reports *5*, 1132-1141.

Heichinger, C., Penkett, C.J., Bahler, J., and Nurse, P. (2006). Genome-wide characterization of fission yeast DNA replication origins. Embo J *25*, 5171-5179.

Hoggard, T., Shor, E., Muller, C.A., Nieduszynski, C.A., and Fox, C.A. (2013). A Link between ORC-origin binding mechanisms and origin activation time revealed in budding yeast. PLoS genetics *9*, e1003798.

Jensen, T.H., Jacquier, A., and Libri, D. (2013). Dealing with pervasive transcription. Molecular cell *52*, 473-484.

Kim, M., Krogan, N.J., Vasiljeva, L., Rando, O.J., Nedea, E., Greenblatt, J.F., and Buratowski, S. (2004). The yeast Rat1 exonuclease promotes transcription termination by RNA polymerase II. Nature *432*, 517-522.

Knott, S.R., Peace, J.M., Ostrow, A.Z., Gan, Y., Rex, A.E., Viggiani, C.J., Tavare, S., and Aparicio, O.M. (2012). Forkhead transcription factors establish origin timing and long-range clustering in S. cerevisiae. Cell *148*, 99-111.

Knott, S.R., Viggiani, C.J., Tavare, S., and Aparicio, O.M. (2009). Genome-wide replication profiles indicate an expansive role for Rpd3L in regulating replication initiation timing or efficiency, and reveal genomic loci of Rpd3 function in Saccharomyces cerevisiae. Genes & development *23*, 1077-1090.

Kubik, S., Bruzzone, M.J., Jacquet, P., Falcone, J.L., Rougemont, J., and Shore, D. (2015). Nucleosome Stability Distinguishes Two Different Promoter Types at All Protein-Coding Genes in Yeast. Molecular cell *60*, 422-434.

Looke, M., Kristjuhan, K., Varv, S., and Kristjuhan, A. (2013). Chromatin-dependent and -independent regulation of DNA replication origin activation in budding yeast. EMBO Rep *14*, 191-198.

Luo, W., Johnson, A.W., and Bentley, D.L. (2006). The role of Rat1 in coupling mRNA 3'-end processing to transcription termination: implications for a unified allosteric-torpedo model. Genes & development *20*, 954-965.

Malabat, C., Feuerbach, F., Ma, L., Saveanu, C., and Jacquier, A. (2015). Quality control of transcription start site selection by nonsense-mediated-mRNA decay. Elife *4*.

Mayan, M.D. (2013). RNAP-II molecules participate in the anchoring of the ORC to rDNA replication origins. PLoS One *8*, e53405.

Mayer, A., di Iulio, J., Maleri, S., Eser, U., Vierstra, J., Reynolds, A., Sandstrom, R., Stamatoyannopoulos, J.A., and Churchman, L.S. (2015). Native elongating transcript sequencing reveals human transcriptional activity at nucleotide resolution. Cell *161*, 541-554.

McGuffee, S.R., Smith, D.J., and Whitehouse, I. (2013). Quantitative, genome-wide analysis of eukaryotic replication initiation and termination. Molecular cell *50*, 123-135.

Miotto, B., Ji, Z., and Struhl, K. (2016). Selectivity of ORC binding sites and the relation to replication timing, fragile sites, and deletions in cancers. Proceedings of the National Academy of Sciences of the United States of America *113*, E4810-4819.

Mori, S., and Shirahige, K. (2007a). Perturbation of the activity of replication origin by meiosis-specific transcription. The Journal of biological chemistry *282*, 4447-4452.

Mori, S., and Shirahige, K. (2007b). Perturbation of the activity of replication origin by meiosis-specific transcription. The Journal of biological chemistry *282*, 4447-4452.

Neil, H., Malabat, C., d'Aubenton-Carafa, Y., Xu, Z., Steinmetz, L.M., and Jacquier, A. (2009). Widespread bidirectional promoters are the major source of cryptic transcripts in yeast. Nature *457*, 1038-1042.

Nieduszynski, C.A., Blow, J.J., and Donaldson, A.D. (2005). The requirement of yeast replication origins for pre-replication complex proteins is modulated by transcription. Nucleic acids research *33*, 2410-2420.

Nieduszynski, C.A., Knox, Y., and Donaldson, A.D. (2006). Genome-wide identification of replication origins in yeast by comparative genomics. Genes & development *20*, 1874-1879.

Nojima, T., Gomes, T., Grosso, A.R., Kimura, H., Dye, M.J., Dhir, S., Carmo-Fonseca, M., and Proudfoot, N.J. (2015). Mammalian NET-Seq Reveals Genome-wide Nascent Transcription Coupled to RNA Processing. Cell *161*, 526-540.

Peace, J.M., Villwock, S.K., Zeytounian, J.L., Gan, Y., and Aparicio, O.M. (2016). Quantitative BrdU immunoprecipitation method demonstrates that Fkh1 and Fkh2 are rate-limiting activators of replication origins that reprogram replication timing in G1 phase. Genome Res *26*, 365-375.

Petryk, N., Kahli, M., d'Aubenton-Carafa, Y., Jaszczyszyn, Y., Shen, Y., Silvain, M., Thermes, C., Chen, C.L., and Hyrien, O. (2016). Replication landscape of the human genome. Nat Commun *7*, 10208.

Porrua, O., Boudvillain, M., and Libri, D. (2016). Transcription Termination: Variations on Common Themes. Trends in genetics : TIG *32*, 508-522.

Preker, P., Nielsen, J., Kammler, S., Lykke-Andersen, S., Christensen, M.S., Mapendano, C.K., Schierup, M.H., and Jensen, T.H. (2008). RNA exosome depletion reveals transcription upstream of active human promoters. Science *322*, 1851-1854.

Pryde, F., Jain, D., Kerr, A., Curley, R., Mariotti, F.R., and Vogelauer, M. (2009). H3 k36 methylation helps determine the timing of cdc45 association with replication origins. PLoS One *4*, e5882.

Raghuraman, M.K., Winzeler, E.A., Collingwood, D., Hunt, S., Wodicka, L., Conway, A., Lockhart, D.J., Davis, R.W., Brewer, B.J., and Fangman, W.L. (2001). Replication dynamics of the yeast genome. Science *294*, 115-121.

Rodriguez, J., Lee, L., Lynch, B., and Tsukiyama, T. (2017). Nucleosome occupancy as a novel chromatin parameter for replication origin functions. Genome Res *27*, 269-277.

Rundlett, S.E., Carmen, A.A., Kobayashi, R., Bavykin, S., Turner, B.M., and Grunstein, M. (1996). HDA1 and RPD3 are members of distinct yeast histone

deacetylase complexes that regulate silencing and transcription. Proceedings of the National Academy of Sciences of the United States of America *93*, 14503-14508.

Schaughency, P., Merran, J., and Corden, J.L. (2014). Genome-wide mapping of yeast RNA polymerase II termination. PLoS genetics *10*, e1004632.

Schulz, D., Schwalb, B., Kiesel, A., Baejen, C., Torkler, P., Gagneur, J., Soeding, J., and Cramer, P. (2013). Transcriptome surveillance by selective termination of noncoding RNA synthesis. Cell *155*, 1075-1087.

Segal, E., and Widom, J. (2009). Poly(dA:dT) tracts: major determinants of nucleosome organization. Current opinion in structural biology *19*, 65-71.

Sequeira-Mendes, J., Diaz-Uriarte, R., Apedaile, A., Huntley, D., Brockdorff, N., and Gomez, M. (2009). Transcription initiation activity sets replication origin efficiency in mammalian cells. PLoS genetics *5*, e1000446.

Snyder, M., Sapolsky, R.J., and Davis, R.W. (1988). Transcription interferes with elements important for chromosome maintenance in Saccharomyces cerevisiae. Mol Cell Biol *8*, 2184-2194.

Soriano, I., Morafraile, E.C., Vazquez, E., Antequera, F., and Segurado, M. (2014). Different nucleosomal architectures at early and late replicating origins in Saccharomyces cerevisiae. BMC genomics *15*, 791.

Soudet, J., Jolivet, P., and Teixeira, M.T. (2014). Elucidation of the DNA end-replication problem in Saccharomyces cerevisiae. Molecular cell *53*, 954-964.

Steinmetz, E.J., Conrad, N.K., Brow, D.A., and Corden, J.L. (2001). RNA-binding protein Nrd1 directs poly(A)-independent 3'-end formation of RNA polymerase II transcripts. Nature *413*, 327-331.

Stinchcomb, D.T., Struhl, K., and Davis, R.W. (1979). Isolation and characterisation of a yeast chromosomal replicator. Nature *282*, 39-43.

Tudek, A., Porrua, O., Kabzinski, T., Lidschreiber, M., Kubicek, K., Fortova, A., Lacroute, F., Vanacova, S., Cramer, P., Stefl, R.*, et al.* (2014). Molecular basis for coordinating transcription termination with noncoding RNA degradation. Molecular cell *55*, 467-481.

Unnikrishnan, A., Gafken, P.R., and Tsukiyama, T. (2010). Dynamic changes in histone acetylation regulate origins of DNA replication. Nat Struct Mol Biol *17*, 430-437.

Uwimana, N., Collin, P., Jeronimo, C., Haibe-Kains, B., and Robert, F. (2017). Bidirectional terminators in Saccharomyces cerevisiae prevent cryptic transcription from invading neighboring genes. Nucleic acids research *45*, 6417-6426.

van Dijk, E.L., Chen, C.L., d'Aubenton-Carafa, Y., Gourvennec, S., Kwapisz, M., Roche, V., Bertrand, C., Silvain, M., Legoix-Ne, P., Loeillet, S.*, et al.* (2011). XUTs are a class of Xrn1-sensitive antisense regulatory non-coding RNA in yeast. Nature *475*, 114-117.

van Nues, R., Schweikert, G., de Leau, E., Selega, A., Langford, A., Franklin, R., Iosub, I., Wadsworth, P., Sanguinetti, G., and Granneman, S. (2017). Kinetic CRAC uncovers a role for Nab3 in determining gene expression profiles during stress. Nat Commun *8*, 12.

Viggiani, C.J., and Aparicio, O.M. (2006). New vectors for simplified construction of BrdU-Incorporating strains of Saccharomyces cerevisiae. Yeast *23*, 1045-1051.

Vogelauer, M., Rubbi, L., Lucas, I., Brewer, B.J., and Grunstein, M. (2002). Histone acetylation regulates the time of replication origin firing. Molecular cell *10*, 1223-1233.

Weiner, A., Hsieh, T.H., Appleboim, A., Chen, H.V., Rahat, A., Amit, I., Rando, O.J., and Friedman, N. (2015). High-resolution chromatin dynamics during a yeast stress response. Molecular cell *58*, 371-386.

Wittmann, S., Renner, M., Watts, B.R., Adams, O., Huseyin, M., Baejen, C., El Omari, K., Kilchert, C., Heo, D.H., Kecman, T.*, et al.* (2017). The conserved protein Seb1 drives transcription termination by binding RNA polymerase II and nascent RNA. Nat Commun *8*, 14861.

Woo, H., Dam Ha, S., Lee, S.B., Buratowski, S., and Kim, T. (2017). Modulation of gene expression dynamics by co-transcriptional histone methylations. Exp Mol Med *49*, e326.

Wyers, F., Rougemaille, M., Badis, G., Rousselle, J.C., Dufour, M.E., Boulay, J., Regnault, B., Devaux, F., Namane, A., Seraphin, B.*, et al.* (2005). Cryptic pol II transcripts are degraded by a nuclear quality control pathway involving a new poly(A) polymerase. Cell *121*, 725-737.

Xu, Z., Wei, W., Gagneur, J., Perocchi, F., Clauder-Munster, S., Camblong, J., Guffanti, E., Stutz, F., Huber, W., and Steinmetz, L.M. (2009). Bidirectional promoters generate pervasive transcription in yeast. Nature *457*, 1033-1037.

Yang, S.C., Rhind, N., and Bechhoefer, J. (2010). Modeling genome-wide replication kinetics reveals a mechanism for regulation of replication timing. Mol Syst Biol *6*, 404.

Yoshida, K., Bacal, J., Desmarais, D., Padioleau, I., Tsaponina, O., Chabes, A., Pantesco, V., Dubois, E., Parrinello, H., Skrzypczak, M.*, et al.* (2014). The histone deacetylases sir2 and rpd3 act on ribosomal DNA to control the replication program in budding yeast. Molecular cell *54*, 691-697.

Yoshida, K., Poveda, A., and Pasero, P. (2013). Time to be versatile: regulation of the replication timing program in budding yeast. J Mol Biol *425*, 4696-4705.

FIGURE LEGENDS

Figure 1: NUTs and CUTs-containing ARS are downregulated when early termination of non-coding RNAs is abrogated.

(A) Numbers and proportions of ARS overlapping with CUTs, NUTs or CUTs/NUTs. ARS annotations used in this study are listed in Supplementary Table 1. **(B)** Scatter dot plot indicating the timing and efficiency of the non-coding RNA-containing ARS (ncARS) compared to replication origins devoid of overlapping ncRNA (Other ARS). Timing and efficiency data were retrieved from Hawkins et al., 2014. **(C)** Nrd1-AA cells were synchronized in G1-phase with alpha-factor during 3 hours at 30°C. During the last hour, rapamycin (Rap) was added or not in the medium. Cells were then washed and released into the cell cycle at 18°C in the presence of BrdU and -/+Rap. After 70min, cells were collected for DNA extraction and BrdU-seq. **(D)** Snapshot depicting a part of chromosome XIII for the BrdU-seq. Affected ARS are indicated in red and non-affected in green. Bottom panel shows a zoom around ARS1320 of the RNA PolII PAR-CLIP in the Nrd1-AA strain (Schaughency et al., 2014). Transcriptional readthrough is indicated by an arrow. **(E)** Plot depicting the mean coverage of BrdU nascent DNA in a 5-Kb window around ACS in -Rap versus +Rap. The 18 red dots and 21 yellow dots represent the ARS showing at least 50% and 35-50% decrease in BrdU incorporation in +Rap respectively. Blue dots represent the ARS defined as non-affected in BrdU incorporation. **(F)** Top: Metagene analysis of the BrdU-seq for the 154 non-affected ARS (<35%) and the 18 most affected ARS (>50%). Profiles represent the mean coverage smoothed by a 200bp-moving window. ARS were oriented according to their ACS T-rich sequence. Bottom: Metagene profiles of the ratio $\log_2$ +Rap/-Rap of the RNA PolII PAR-CLIP signal 500bp around the oriented ACS of the least and most affected ARS (Schaugency et al., 2014). Plots were smoothed by a 20bp-moving window. Since ARS are oriented, nascent transcription going towards replication origins is defined as Sense and Antisense. The grey box represents the window in which transcriptional readthrough was analyzed in Figure 1G. **(G)** Scatter dot-plots representing the ratio $\log_2$ +Rap/-Rap of the RNA PolII PAR-CLIP signal over the

3 classes of ARS defined in Figure 1E. Total nascent transcription in +Rap and –Rap was defined on oriented ARS by adding the RNA PolII PAR-CLIP mean densities between the ACS to +100bp on the sense strand to the signal over the same region on the antisense strand in each condition using the data from Schaughency et al., 2014. Each 100bp segment was considered as 1 bin (See Materials and Methods).

Figure 2: Non-coding transcription readthrough into replication origins alters nucleosome occupancy.

(A) Metagene analysis of MNase-seq from Nrd1-AA cells treated or not with rapamycin for 1h at the 3 classes of ARS defined in Figure 1. The grey box represents the window in which transcriptional readthrough was analyzed. **(B)** Scatter dot plot representing the difference of coverage (Δcoverage) between the ACS to +100 of oriented ARS when comparing +Rap and –Rap conditions. **(C)** Snapshot of the MNase-seq around ARS420 belonging to the class of most affected ARS.

Figure 3: Natural pervasive transcription correlates with timing/efficiency and specific chromatin features of replication origins.

(A) Metagene analysis of Sense and Antisense RNA PolII PAR-CLIP (Schaughency et al., 2014) and **(B)** RNA-seq (Uwimana et al., 2017) data in the vicinity of 266 oriented replication origins. Data were smoothed by a 20bp-moving window. The grey box represents the window in which transcriptional readthrough was analyzed. **(C)** The 266 replication origins were divided into 2 classes according to their level of total natural readthrough transcription (High or Low). This basal nascent transcription was calculated on oriented ARS by adding the RNA PolII PAR-CLIP mean densities between the ACS and +100bp on the sense strand to the signal over the same region on the antisense strand. Each 100bp segment was considered as 1 bin. Natural nascent transcription data were taken from Schaugency et al., 2014. **(D)** Replication timing and efficiency of the 2 classes of ARS defined as in (C). **(E)(F)(G)(H)** Nucleosome positioning, H3K36me3, H3K18ac and ORC levels considering the 2 classes of replication origins**.** Data for

nucleosome positioning, histone marks and ORC recruitment were retrieved from Kubik et al., 2016; Weiner et al., 2015 and Belsky et al., 2015 respectively. For these plots, ARS were oriented and aligned according to their ACS T-rich sequence.

Figure 4: mRNA termination readthrough at replication origins leads to chromatin remodeling and decreased ORC binding.

(A) Experimental scheme as described in Figure 1C. **(B)** Plot depicting the mean coverage of BrdU nascent DNA over the same 193 ARS as in Figure 1E. The 29 red dots and 164 blue dots represent the ARS showing >80% and <80% decrease in BrdU incorporation in +Rap versus -Rap respectively. **(C)** Scatter dot-plots representing the ratio $\log_2$ +Rap/-Rap of the RNA PolII PAR-CLIP signal from both strands between the ACS and +100 of oriented ARS in the Ysh1-AA strain at the 2 classes of ARS defined above. **(D)** Heat map representing the fold change of transcriptional readthrough at replication origins in the Ysh1-AA mutant. The 193 ARS were classified according to their configuration (defined by the presence or absence of a gene within the 500bp surrounding the ACS) and ranked by their total readthrough increase on the ACS to +100bp. The 3 ARS indicated in red have high levels of total readthrough, belong to the >80% class defined in Figure 4B and were chosen for the following experiments. The ARS depicted in green show mid or low total readthrough, belong to the <80% class and have been used as controls for the following experiments. **(E)(F)(G)(H)** Chromatin immunoprecipitation (ChIP) of H3, H3K36me3, H3K18ac and ORC at ARS with high (red) and low (green) readthrough transcription. Asynchronous cells were treated 30min with rapamycin to induce Ysh1 depletion from the nucleus and ChIP was performed as described in Materials and Methods. Immunoprecipitated ARS loci were normalized to immunoprecipitated *SPT15* ORF after qPCR amplification. Fold enrichment was artificially set to 1 for the – Rap condition (n=3). Error bars represent Standard Error of the Mean (SEM).

Figure 5: Absence of Set2 H3K36 methyl transferase partially rescues replication defects due to non-coding transcription readthrough.

(A) Experimental scheme as described in Figure 1C. **(B)** Metagene analysis of the BrdU-seq for the 154 non-affected ARS (<35%) and the 18 most affected ARS (>50%) for the Nrd1-AA and Nrd1-AA *set2Δ* strains. Plots for the Nrd1-AA strain were already presented in Figure 1F with the exception of the Normalized coverage for which calculation is detailed in Materials and Methods. Profiles represent the mean coverage smoothed by a 200bp-moving window. ARS were oriented according to their ACS T-rich sequence. **(C)** Scatter dot plot presenting the normalized BrdU ratio for the different classes of ARS affected in BrdU incorporation in an Nrd1-AA strain and for the same classes of ARS in the Nrd1-AA *set2Δ* strain. **(D)** Snapshot depicting the BrdU-seq reads for a part of chromosome XIII. ARS that are rescued in BrdU incorporation in the Nrd1-AA *set2Δ* +Rap condition are depicted in red while non-affected ARS are in green. **(E)** Metagene analysis of BrdU incorporation 5Kb around non-replicating ACS (nr-ACS) in the indicated strains grown in –/+Rap. The representation is smoothed over a 200bp-moving window. **(F)** Snapshot illustrating the activation of a dormant nr-ACS in the Nrd1-AA *set2Δ* +Rap condition.

Figure 6: Pervasive transcription influences replication timing/efficiency by modulating ARS chromatin structure and ORC binding.

The chromatin structure of replication origins is defined, at least in part, by the level of pervasive readthrough transcription. In the presence of efficient non-coding (Nrd1/Nab3/Sen1-dependent) or mRNA (CPF/CF-dependent) transcription termination, ARS present low H3K36 trimethylation, high histone acetylation (Ac), a wide NDR and more ORC binding at the ACS, favoring early and efficient replication. If transcription termination is deficient, H3K36me3 by Set2 increases and histone acetylation decreases likely through the recruitment of the Rpd3 histone deacetylase; these modifications increase nucleosome stability and occupancy over the ARS, lowering the level of ORC recruitment and resulting in late and inefficient ARS replication.

Supplementary Figure 1: related to Figure 1.

(A) Configuration distributions of the 57 ncRNAs-containing ARS (ncARS) with respect to the ACS. **(B)** FACS profiles of S-phase progression for the Nrd1-AA strain. **(C)** The mean coverage of BrdU nascent DNA in a 5Kb window centered around the ACS was measured for the 193 ARS taken into account in Figure 1E. The plots represent this mean coverage for the 2 replicates in either –Rap or +Rap. **(D)** Heatmap representing the BrdU-seq densities (log_2) 20Kb around the ACS of the 193 replication origins considered as active in the experiment. **(E)** Overlap between the 57 ncRNA-containing ARS and the different classes of BrdU incorporation-defective replication origins in +Rap versus -Rap. The ncARS strongly overlap with the most affected ARS.

Supplementary Figure 2: related to Figure 1.

(A) Rrp6-AA cells were treated as in Figure 1C. RNA was extracted in G1-phase while DNA extraction and BrdU immunoprecipitation were performed at the 80 min time point following release into S-phase. **(B)** FACS profiles of S-phase progression for the Rrp6-AA strain. **(C)** RT-qPCR analysis of CUTs-containing ARS in G1-phase synchronized cells with or without 1h rapamycin treatment. Measured ncRNAs were normalized to *SCR1* RNA. **(D)** Analysis of BrdU incorporation after 80 min of S-phase release at 18°C. Three ARS which do not contain CUTs were used as controls. Fold enrichment represents the ratio of immunoprecipitated BrdU for a given ARS over the value of the very late replicated origin ARS609. For **(C)** and **(D)**, the fold enrichment was artificially set to 1 for the –Rap condition (n=3). Error bars represent SEM.

Supplementary Figure 3: related to Figure 3.

(A) Gene configuration around All ARS, Highly and Lowly transcribed ARS. A gene was considered as convergent if pointing to the ARS within a distance <500bp to the ACS. **(B)** Scatter dot plot of nascent transcription pointing toward the ARS either Upstream (-400 to -300bp) or Downstream (+400 to +500bp) relative to the oriented ACS. **(C)** Scatter dot plot representing natural

readthrough of CUTs/NUTs-containing ARS (ncARS) versus High and Low classes. **(D)** Scatter dot plot presenting nascent transcription in the ACS to +100bp region for ORC-bound ACS (ORC-ACS) and non-replicated ACS (nrACS) as defined in Eaton et al., 2010.

Supplementary Figure 4: related to Figure 3.

(A)(B)(C)(D) Metagene analysis of the H3K14ac, H4K12ac, H4K5ac and H3K4me2 profiles around the ACS of the 43 ARS with High and 223 ARS with Low readthrough transcription. Data were retrieved from (Weiner et al., 2015). Results were smoothed over a 20bp-moving window.

Supplementary Figure 5: related to Figure 4.

(A) FACS analysis of the Ysh1-AA strain. Cells were treated as shown in Figure 4A. **(B)** Upper panel: Metagene analysis of BrdU incorporation in the Ysh1-AA strain for the 193 ARS defined as incorporating BrdU in our study (see Suppl. Figure 1D). The plot was smoothed with a 200bp-moving window. Bottom panel: Metagene analysis of the RNA PolII PAR-CLIP in the Ysh1-AA strain. Profiles are presented as the log2 ratio +Rap/-Rap for either Sense or Antisense nascent transcription relative to the oriented ACS data (Schaughency et al., 2014). The profile was smoothed over a 20bp-moving window. The grey box represents the window in which transcriptional readthrough was analyzed. **(C)** Top: Snapshot illustrating the BrdU incorporation defect in the Ysh1-AA strain. Bottom: zoom over the ARS209 showing the *HHF1* gene readthrough transcription over the ACS by RNA PolII PAR-CLIP. Transcriptional readthrough is indicated by an arrow.

Supplementary Figure 6: related to Figure 4.

(A) Heat map representing the fold change of transcriptional readthrough at replication origins in the Nrd1-AA strain. The 193 ARS were classified according to their defects in BrdU incorporation (see Figure 1E and G) and ranked by their total readthrough increase over the ACS to +100bp area. The 3 ARS indicated in red have high levels of total readthrough. The ARS depicted in green show mild or low total readthrough. **(B)(C)(D)** ChIP of H3, H3K36me3 and H3K18ac at ARS

with high (red) and low (green) readthrough. Asynchronous cells were treated 1h with rapamycin to induce Nrd1 depletion from the nucleus and ChIP was performed as described in Materials and Methods. Immunoprecipitated ARS loci were normalized to immunoprecipitated *SPT15* ORF after qPCR amplification. Fold enrichment was artificially set to 1 for the –Rap condition (n=3). Error bars represent Standard Error of the Mean (SEM).

Supplementary Figure 7: related to Figure 5.

(A) FACS analysis of the Nrd1-AA *set2Δ* strain. Cells were treated as shown in Figure 5A. **(B)** RT-qPCR analysis of NUTs-containing ARS in the Nrd1-AA and Nrd1-AA *set2Δ* strains with or without 1h rapamycin treatment. Measured ncRNAs were normalized to *SCR1* RNA.

Supplementary Table 1. List of ARS features used in this study

Chr	ACS	ARS	Orientation	Timing (min)	Efficiency (%)
chrI	147536	ARS108	-	23.7347	0.667998741678771
chrI	124521	ARS107	-	27.4037	0.740703497521513
chrI	70432	ARS106	-	31.2909	0.21809657955213
chrI	31003	ARS104	+	4.96419	0.0719520488939761
chrI	176233	ARS110	+	25.3717	0.0712395625914559
chrI	42059	ARS105	+	28.6596	0.326040263743236
chrII	237875	ARS208	-	15.5877	0.694864245560776
chrII	63373	ARS202	-	19.0662	0.615570807123544
chrII	486897	ARS216	-	19.9821	0.760479870181951
chrII	255081	ARS209	-	24.9689	0.501250041721504
chrII	418010	ARS215	-	25.2669	0.488220153184766
chrII	774020	ARS227	-	27.5495	0.430912528518724
chrII	802270	ARS229	-	28.1188	0.588447645217387
chrII	170263	ARS207	-	31.7143	0.376993437322729
chrII	408041	ARS214	-	34.8444	0.391047358307991
chrII	622754	ARS220	+	21.2722	0.699719913338349
chrII	326193	ARS211	+	27.1654	0.765760622361523
chrII	632018	ARS221	+	29.1283	0.300892998193591
chrII	611771	ARS219.5	+	32.3319	0.255222301990781
chrIII	30441	ARS304	-	8.11	0.0483124418941826
chrIII	39591	ARS305	-	16.2378	0.590598012716755
chrIII	108972	ARS307	-	17.5676	0.344517443487245
chrIII	114613	ARS308	-	31.0834	0.0444790554234571
chrIII	74523	ARS306	+	14.5006	0.77676468159701
chrIII	224858	ARS315	+	17.4523	0.837005358732442
chrIII	166657	ARS310	+	18.1581	0.409472090947731
chrIII	132042	ARS309	+	21.817	0.542510294429072
chrIII	315816	ARS319	+	23.1442	0.246806812854223
chrIV	484036	ARS417	-	16.8337	0.536441888989149
chrIV	555399	ARS418	-	17.2337	0.923752585379454
chrIV	1159443	ARS432	-	18.662	0.4780935727447
chrIV	1166175	ARS432.5	-	19.2007	0.64414328872031
chrIV	462597	ARS416	-	19.4968	0.108481301559666
chrIV	1302759	ARS435	-	20.0158	0.704104468911277
chrIV	505519	ARS417.5	-	20.8379	0.562168906581161
chrIV	329742	ARS413	-	21.9365	0.660397771981137
chrIV	1502772	ARS447	-	25.2917	0.0517316261057703
chrIV	212593	ARS409	-	29.5497	0.558134837880863
chrIV	46222	ARS404	-	30.0596	0.667634369019351
chrIV	567679	ARS419	-	31.2064	0.125632918605979
chrIV	629309	ARS420	-	31.7754	0.587146509361626

chrIV	640065	ARS421	-	34.6259	0.414818079479181
chrIV	1461904	ARS442	+	19.0736	0.278007694913019
chrIV	408132	ARS414	+	20.703	0.374031842615967
chrIV	913862	ARS428	+	21.3407	0.400628137004749
chrIV	921742	ARS429	+	21.5721	0.242533962498067
chrIV	316878	ARS412	+	24.3647	0.288640824018793
chrIV	123677	ARS406	+	27.2451	0.512217924096682
chrIV	1057893	ARS431	+	29.5874	0.505820120108683
chrIX	73953	ARS907	-	19.8883	0.349791492098066
chrIX	105966	ARS909	-	21.9717	0.790398309499989
chrIX	412000	ARS922	-	22.1491	0.66001390938269
chrIX	342028	ARS919	-	27.0509	0.578692679731482
chrIX	310739	ARS916	-	30.6601	0.557296129252782
chrIX	214733	ARS913	+	15.8712	0.642997853853591
chrIX	175171	ARS912	+	26.3445	0.627632757375481
chrIX	357223	ARS920	+	26.4734	0.603907721511652
chrIX	80373	ARS908	+	28.2147	0.412840301984809
chrV	173807	ARS511	-	18.7794	0.88989955955209
chrV	59469	ARS507	-	19.6204	0.797953717350464
chrV	145713	ARS510	-	19.6512	0.582663382795232
chrV	406902	ARS517	-	19.9773	0.881138953410136
chrV	94056	ARS508	+	17.2505	0.913874252641905
chrV	353583	ARS516	+	20.327	0.832855303710458
chrV	569630	ARS523	+	21.305	0.402771194252224
chrV	287566	ARS514	+	26.3212	0.501511923560309
chrV	212455	ARS512	+	26.8156	0.727278375165151
chrV	498900	ARS520	+	27.7409	0.75778642705041
chrV	549586	ARS522	+	30.0717	0.371784229941525
chrVI	167731	ARS606	-	20.2874	0.755577774153215
chrVI	118678	ARS603.5	-	26.9612	0.556089665736437
chrVI	5479	ARS600.1	-	35.0366	0.0676515181557582
chrVI	136037	ARS605	-	36.2767	0.246643518016851
chrVI	104557	ARS603.1	-	36.561	0.0917743837667637
chrVI	199402	ARS607	+	15.3775	0.936330493374592
chrVI	127869	ARS604	+	19.365	0.298832270187241
chrVI	68832	ARS603	+	25.8027	0.658623712112408
chrVI	216470	ARS608	+	49.0724	0.00268103836860201
chrVII	485115	ARS719	-	16.8899	0.771071395904932
chrVII	834669	ARS731	-	17.1742	0.859734144435557
chrVII	508911	ARS720	-	19.3455	0.463993923009539
chrVII	653836	ARS726	-	19.5283	0.603397532826508
chrVII	388849	ARS717	-	20.5614	0.772919848889663
chrVII	977910	ARS733	-	21.6756	0.608210438042281
chrVII	421285	ARS718	-	21.7473	0.8254030328801
chrVII	352866	ARS716	-	25.9853	0.716693102334425
chrVII	64458	ARS702	-	30.0013	0.633267922343479

chrVII	660004	ARS727	-	31.9788	0.334956684425253
chrVII	17906	ARS700.5	-	33.2508	0.293930239292816
chrVII	1083677	ARS131a	+	17.1759	0.268320993336173
chrVII	888418	ARS731.5	+	17.6026	0.785674896656648
chrVII	715319	ARS728	+	21.3856	0.802675358290452
chrVII	163242	ARS707	+	23.7287	0.666488449451596
chrVII	203978	ARS710	+	32.8392	0.465627057123858
chrVIII	392250	ARS818	-	20.1333	0.461723419325449
chrVIII	501949	ARS822	-	20.4363	0.657013950795127
chrVIII	447794	ARS820	-	20.8906	0.891279693338375
chrVIII	359698	ARS816	-	21.3874	0.699420993453168
chrVIII	45778	ARS804	-	27.4092	0.215813246196311
chrVIII	297102	ARS815	+	19.6499	0.908223153207234
chrVIII	64301	ARS805	+	21.111	0.63666787078685
chrVIII	168599	ARS809	+	23.8383	0.562781552726125
chrVIII	245791	ARS813	+	25.611	0.834390876136793
chrVIII	556152	ARS824	+	38.3945	0.163454097251403
chrX	7724	ARS1002	-	14.135	0.0951563044067678
chrX	417311	ARS1014	-	18.0605	0.769152826232888
chrX	654465	ARS1020	-	20.441	0.482594264187954
chrX	442416	ARS1015	-	22.2691	0.270562375299879
chrX	113736	ARS1007	-	22.7052	0.661819330549483
chrX	67713	ARS1005	-	24.2489	0.833786787715688
chrX	228567	ARS1009	-	26.895	0.448599115528679
chrX	374861	ARS1012	+	16.8433	0.790062380466916
chrX	683928	ARS1021	+	21.2419	0.836374474222757
chrX	161448	ARS1007.5	+	22.882	0.678928231914171
chrX	99507	ARS1006	+	44.8774	0.0681145404602845
chrXI	55867	ARS1103	-	20.4597	0.858679740249766
chrXI	329502	ARS1109	-	23.609	0.669165975609654
chrXI	213310	ARS1106.7	-	24.5627	0.610637864267786
chrXI	153125	ARS1106	-	24.7737	0.741777084425719
chrXI	457168	ARS1114.5	-	26.9254	0.385768370555651
chrXI	612053	ARS1120	-	27.4193	0.659963827297213
chrXI	388668	ARS1112	+	23.7751	0.70792633433261
chrXI	98390	ARS1104.5	+	23.9434	0.805550469052816
chrXI	257590	ARS1107	+	24.5643	0.823267553602652
chrXI	642422	ARS1123	+	24.8322	0.285126326157317
chrXI	416884	ARS1113	+	27.8218	0.507542824198083
chrXII	373328	ARS1213	-	16.1652	0.924071376240351
chrXII	513085	ARS1217	-	18.7291	0.928716953757194
chrXII	412853	ARS1215	-	20.842	0.791304264711981
chrXII	794192	ARS1226	-	21.5847	0.72433410250391
chrXII	231251	ARS1211	+	18.4432	0.885869886627941
chrXII	1007238	ARS1232	+	22.0498	0.653238997985624
chrXII	659895	ARS1220	+	23.2991	0.615907057558801

chrXII	730540	ARS1222	+	24.0344	0.616976262415629
chrXII	156701	ARS1209	+	27.6889	0.106583180140746
chrXII	243743	ARS1211.5	+	31.5381	0.194891632601611
chrXII	622861	ARS1219	+	31.9128	0.21804039777797
chrXII	1013787	ARS1233	+	34.9386	0.205599911012952
chrXIII	503627	ARS1319	-	18.955	0.693079561277871
chrXIII	535769	ARS1320	-	20.8635	0.787538325387696
chrXIII	94390	ARS1305	-	22.5112	0.759219728490202
chrXIII	554598	ARS1322	-	23.1905	0.350950315672886
chrXIII	897975	ARS1332	-	25.7874	0.812339223688561
chrXIII	40132	ARS1304	-	30.0956	0.243440083269417
chrXIII	758416	ARS1327	-	31.0105	0.568880592135122
chrXIII	815391	ARS1330	+	18.7283	0.702257277815255
chrXIII	31767	ARS1303	+	20.1238	0.346139505494882
chrXIII	263127	ARS1309	+	20.7798	0.588813043615569
chrXIII	634521	ARS1324	+	21.2954	0.448636262993266
chrXIII	433030	ARS1315	+	21.6495	0.590410906657223
chrXIII	137322	ARS1307	+	21.6644	0.674907434726042
chrXIII	805162	ARS1329	+	23.1108	0.409585840622337
chrXIII	371020	ARS1312	+	23.2419	0.831510616402894
chrXIII	649362	ARS1325	+	23.8334	0.570393948825248
chrXIII	159062	ARS1307.5	+	27.3582	0.438228752220384
chrXIII	611318	ARS1323	+	33.9865	0.478851049624177
chrXIV	89756	ARS1407	-	22.4982	0.673307914816788
chrXIV	280067	ARS1414	-	23.015	0.690494121057685
chrXIV	691682	ARS1427	-	23.6753	0.671950152749659
chrXIV	635835	ARS1426	-	26.3996	0.508902068891593
chrXIV	412443	ARS1417	-	27.8787	0.727452906306385
chrXIV	546150	ARS1421	-	28.9553	0.351773918443852
chrXIV	449538	ARS1419	-	30.2685	0.616086907882604
chrXIV	322006	ARS1415	+	20.9471	0.779723812980731
chrXIV	609538	ARS1424	+	23.7391	0.778533383908303
chrXIV	499042	ARS1420	+	25.4344	0.725115781824161
chrXIV	61696	ARS1406	+	28.9452	0.584343663450139
chrXV	277733	ARS1511	-	19.3531	0.889202415060848
chrXV	309249	ARS1512	-	19.7621	0.424077556767852
chrXV	874369	ARS1526	-	22.9549	0.61555518465665
chrXV	155258	ARS1509.5	-	28.3077	0.165319456525643
chrXV	337484	ARS1513	-	31.2743	0.388633693848768
chrXV	85360	ARS1508	-	31.364	0.340508496476595
chrXV	167004	ARS1510	+	21.679	0.78784289224592
chrXV	113910	ARS1509	+	22.0656	0.745961065608586
chrXV	766691	ARS1523	+	23.198	0.76686652591733
chrXV	436793	ARS1513.5	+	24.7319	0.61006807653897
chrXV	72689	ARS1507	+	25.6447	0.58121517123004
chrXV	908311	ARS1528	+	33.9907	0.277709945035728

chrXV	35714	ARS1506.5	+	34.0243	0.199229573718266
chrXVI	777096	ARS1626.5	-	17.9451	0.837915202652846
chrXVI	43150	ARS1604	-	19.9309	0.16956178908746
chrXVI	695620	ARS1625	-	25.2799	0.688862961374123
chrXVI	842852	ARS1628	-	33.0415	0.415454264708472
chrXVI	933166	ARS1631	-	41.2433	0.0084433642640322
chrXVI	7171	ARS1601	-	49.8567	0.106873088445925
chrXVI	289531	ARS1614	+	18.2715	0.622532483168324
chrXVI	73105	ARS1605	+	20.3504	0.744583753905223
chrXVI	384595	ARS1618	+	20.9913	0.559576096002154
chrXVI	633924	ARS1623	+	21.1529	0.894941644869243
chrXVI	511707	ARS1621	+	22.7185	0.693415651617847
chrXVI	116594	ARS1607	+	23.3578	0.636107495835738
chrXVI	684408	ARS1624	+	31.8878	0.332866228524324
chrI	215011	ARS111	-	18.7795	0.669558212817115
chrI	6572	ARS201	-	26.7142	0.379405656891252
chrII	539400	ARS218	-	18.3388	0.355591002245284
chrII	517285	ARS217	-	22.38	0.192092825302214
chrII	143692	ARS206	-	26.3513	0.586386970527371
chrII	741781	ARS224	-	28.2181	0.52053805374326
chrII	591434	ARS219	+	18.5753	0.446851201760138
chrII	676302	ARS221.5	+	21.9239	0.116918700996598
chrII	93553	ARS203	+	22.0683	0.315086307185498
chrII	379119	ARS212	+	26.9637	0.385823534297593
chrII	757485	ARS225	+	30.9973	0.31933327428219
chrIII	273027	ARS316	-	22.4159	0.464768766652256
chrIII	1062	ARS300	-	47.9548	0.0334722941658927
chrIV	21745	ARS402.5	-	12.9027	0.141228995783595
chrIV	1033263	ARS430.5	-	16.1357	0.433607033642221
chrIV	236050	ARS409.5	-	20.5995	0.681356620001321
chrIV	101241	ARS405.5	-	21.7059	0.470592940366211
chrIV	1487095	ARS446	-	24.1319	0.453880443588644
chrIV	852	ARS400	-	25.9882	0.565837318325764
chrIV	15681	ARS403	-	26.4963	0.126347448699275
chrIV	1110136	ARS431.5	-	27.7114	0.628632467019032
chrIV	86124	ARS405	-	42.9028	0.189014968184954
chrIV	351162	ARS413.5	+	7.17173	0.124550108563836
chrIV	702929	ARS422	+	21.481	0.70087921608329
chrIV	1404327	ARS440	+	22.3676	0.489300604917536
chrIV	1276272	ARS434	+	27.1883	0.65143967775415
chrIV	1240924	ARS433	+	27.5127	0.820429897985069
chrIV	845128	ARS426.5	+	28.4031	0.35872781445972
chrIV	253841	ARS410	+	29.9722	0.183043101299049
chrIX	136287	ARS911	-	22.4781	0.560953090716211
chrIX	163115	ARS911.5	-	32.7857	0.112343129808842
chrV	520952	ARS521	+	30.8507	0.391670761289066

chrVI	12805	ARS600.2	-	48.2677	0.0260192696915216
chrVII	241201	ARS712	+	13.008	0.0979957430390257
chrVII	187407	ARS709	+	28.5936	0.393901217349225
chrVII	1063520	ARS735.5	+	33.9172	0.579700418735279
chrVIII	535621	ARS823.5	-	28.8842	0.540185736225325
chrVIII	520379	ARS823	-	46.0398	0.144821598426995
chrX	248881	ARS1009.5	-	23.4482	0.113366278612888
chrX	737125	ARS1024	-	47.6708	0.0965090541424323
chrX	730035	ARS1023	+	17.4862	0.195597730930874
chrX	337270	ARS1011	+	20.0571	0.494195864550591
chrX	16474	ARS1003	+	24.3374	0.0533345441020337
chrX	298838	ARS1010	+	25.8883	0.678079244822445
chrX	711883	ARS1022	+	40.7325	0.112008773500507
chrX	23928	ARS1004	+	48.7468	0.337229155218381
chrXII	52108	ARS1203	-	24.8856	0.337486877170992
chrXII	888740	ARS1227.5	-	25.101	0.76812817379299
chrXII	289421	ARS1212	-	28.6952	0.683635067618034
chrXII	1024153	ARS1234	-	29.3942	0.408994417094092
chrXII	822105	ARS1227	+	28.4606	0.668248116490512
chrXIII	468237	ARS1316	+	23.3442	0.44141776901299
chrXIII	688918	ARS1326	+	28.5139	0.39242487957153
chrXIII	878735	ARS1331.7	+	30.6401	0.261659852738096
chrXIII	772677	ARS1328	+	32.1779	0.310037045140512
chrXIII	865471	ARS1331.5	+	49.2252	0.00624534501447316
chrXIV	250465	ARS1413	-	25.5025	0.530053921423613
chrXIV	764337	ARS1429	-	26.0257	0.415849671209073
chrXIV	169749	ARS1411	-	27.6023	0.621713876624478
chrXIV	196226	ARS1412	-	31.1475	0.626432110857976
chrXIV	28653	ARS1405	-	31.6981	0.0366203907948347
chrXIV	126679	ARS1410	-	37.7627	0.342016625465444
chrXIV	738730	ARS1428.5	+	35.2375	0.442055784809562
chrXV	520953	ARS1515.7	-	11.525	0.0179804407174783
chrXV	566598	ARS1516	-	21.6888	0.780259104695094
chrXV	681350	ARS1520	-	29.1629	0.622378275092329
chrXV	729797	ARS1521	+	19.4475	0.3160513018827
chrXV	783388	ARS1524	+	22.5625	0.345902444500802
chrXV	656703	ARS1519	+	26.4714	0.632392265446849
chrXVI	584397	ARS1622.7	-	29.0811	0.258870553023387
chrXVI	331771	ARS1617	+	23.2352	0.477311632567126
chrXVI	880921	ARS1630	+	30.5296	0.613328928370058
chrXVI	749120	ARS1626	+	36.4613	0.0463496399503821

* The 193 ARS analyzed for BrdU incorporation (Figures 1, 4 and 5) are indicated in grey.

Supplementary Table 2. List of strains used in this study

Strain	Lab name	Genotype
Nrd1-AA	FSY5348	*MAT a, tor1-1, fpr1::NAT, RPL13A-2×FKBP12::TRP1, NRD1-FRB::KanMX6, bar1::LEU2, BrdU-inc::HIS3, ura3-1, ade2-1*
Nrd1-AA *set2Δ*	FSY7284	*MAT a, tor1-1, fpr1::NAT, RPL13A-2×FKBP12::TRP1, NRD1-FRB::KanMX6, bar1::LEU2, BrdU-inc::HIS3, set2 ::URA3, ade2-1*
Rrp6-AA	FSY5725	*MAT a, tor1-1, fpr1::loxP-LEU2-loxP, RPL13A-2×FKBP12::loxP, RRP6-FRB::KanMX6, bar1::URA3, BrdU-inc::HIS3, ade 2-1 trp1-1, leu2-3,112*
Ysh1-AA	FSY7715	*MAT a, tor1-1, fpr1::loxP-LEU2-loxP, RPL13A-2×FKBP12::loxP, YSH1-FRB::KanMX6, bar1::URA3, BrdU-inc::HIS3, ade 2-1 trp1-1, leu2-3,112*

Figure 1

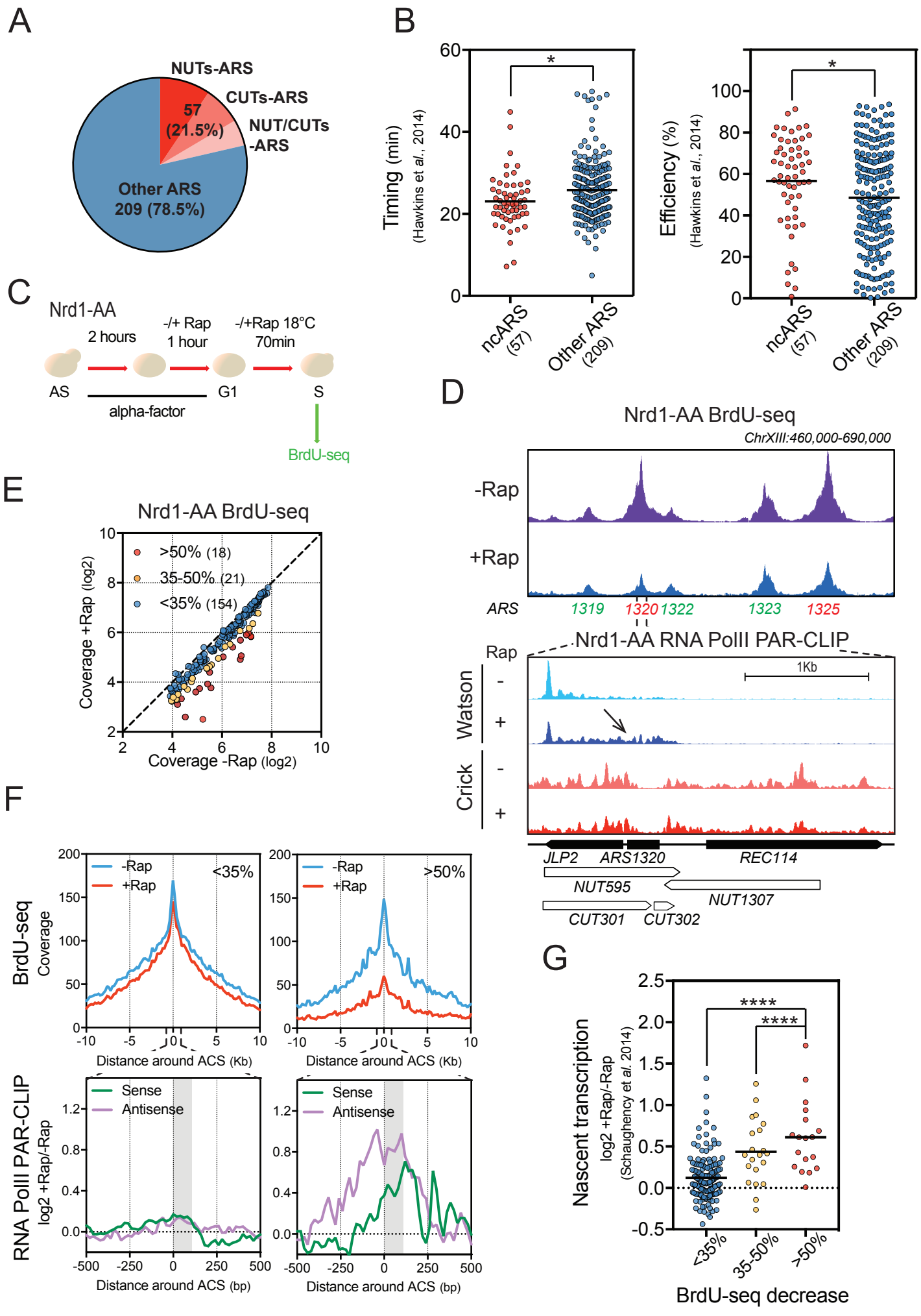

Figure 2

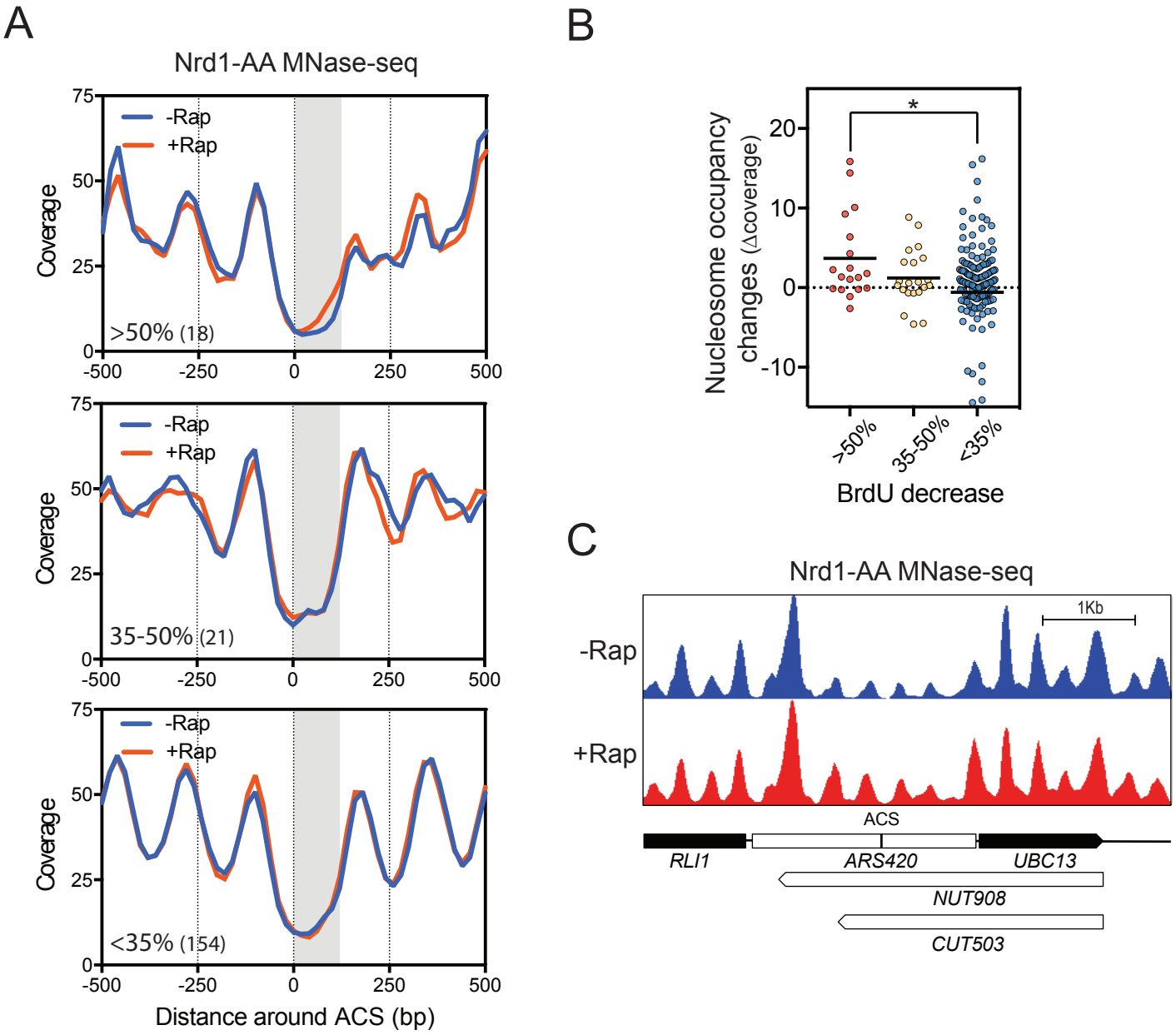

Figure 3

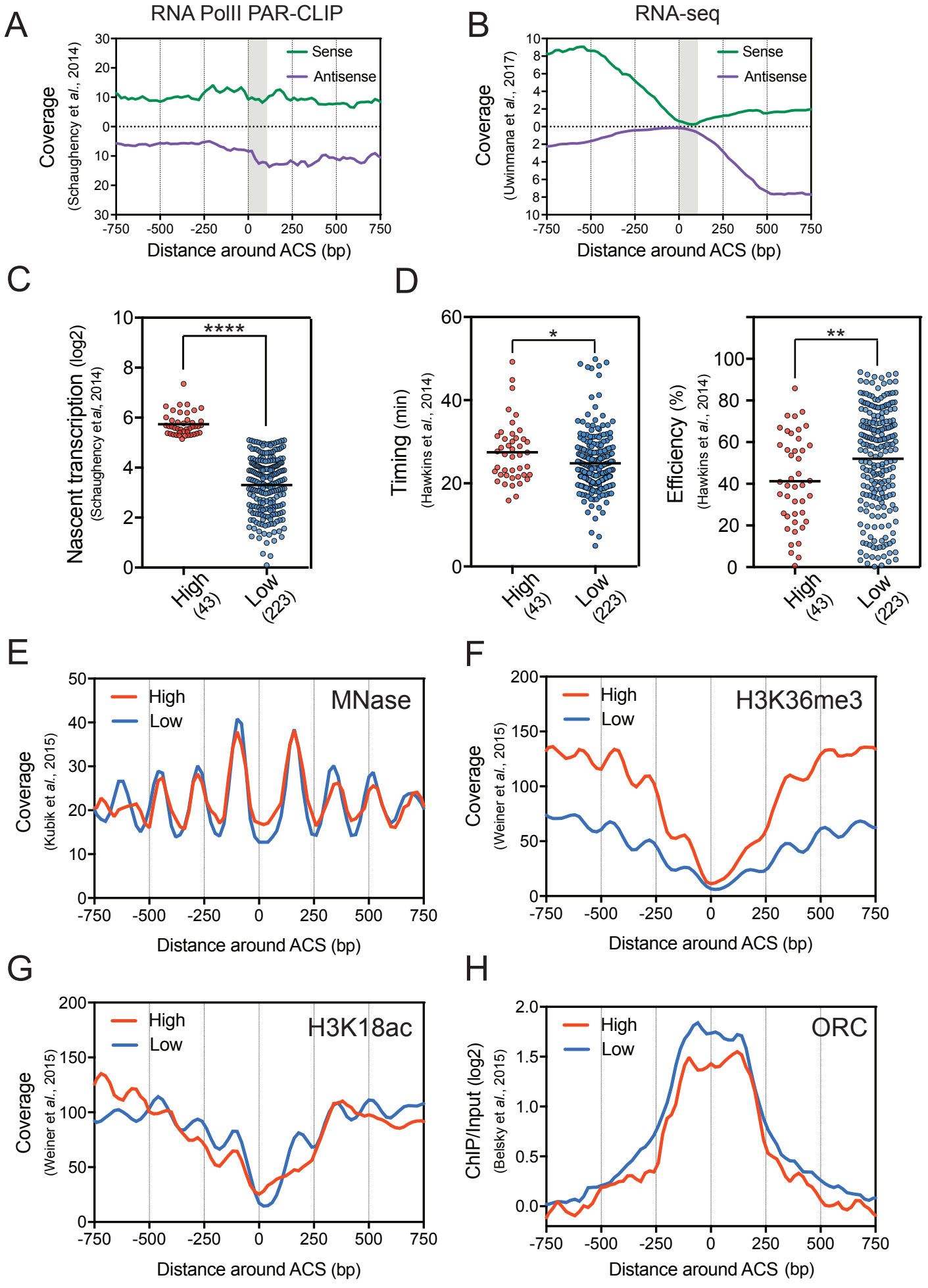

Figure 4

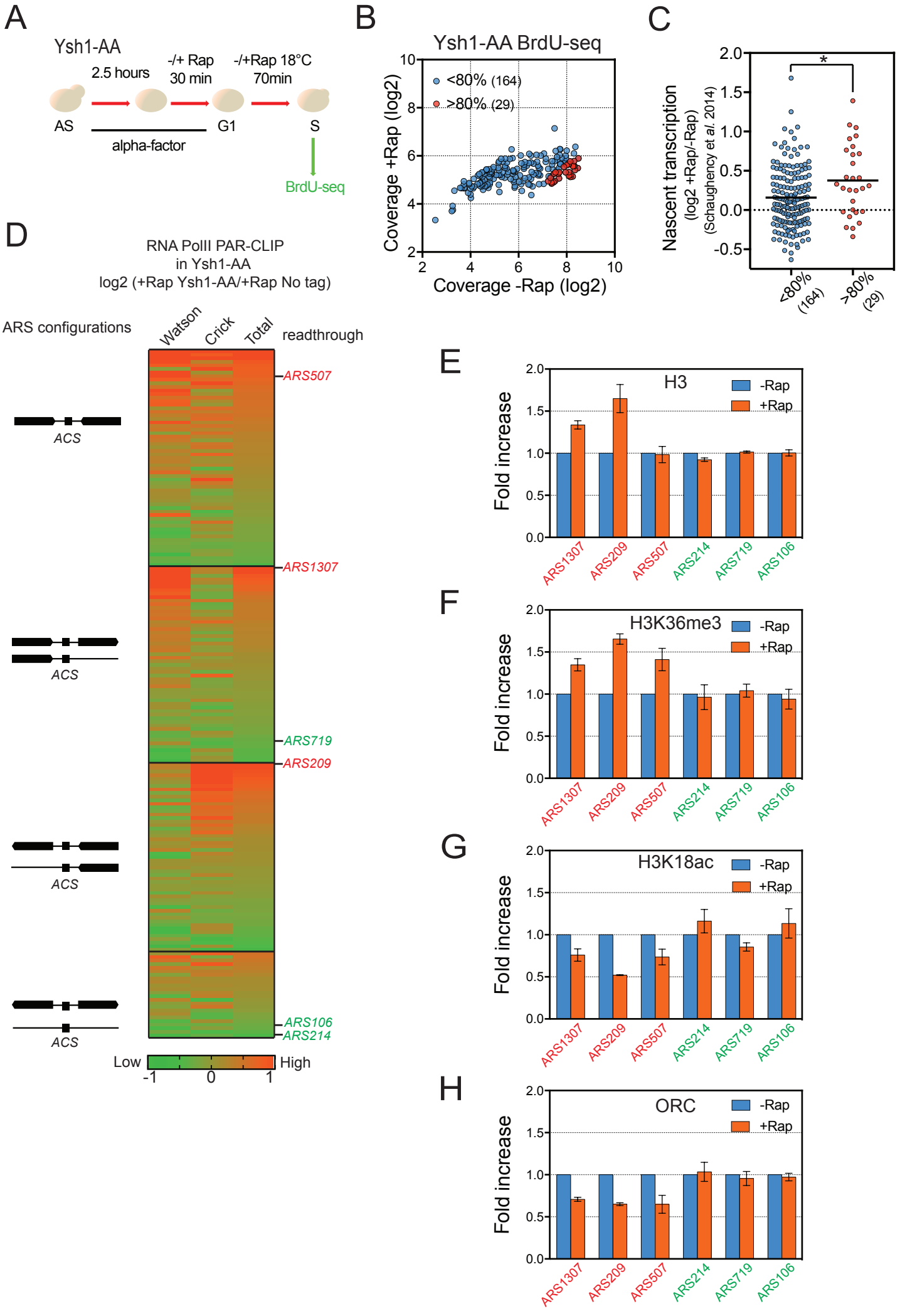

Figure 5

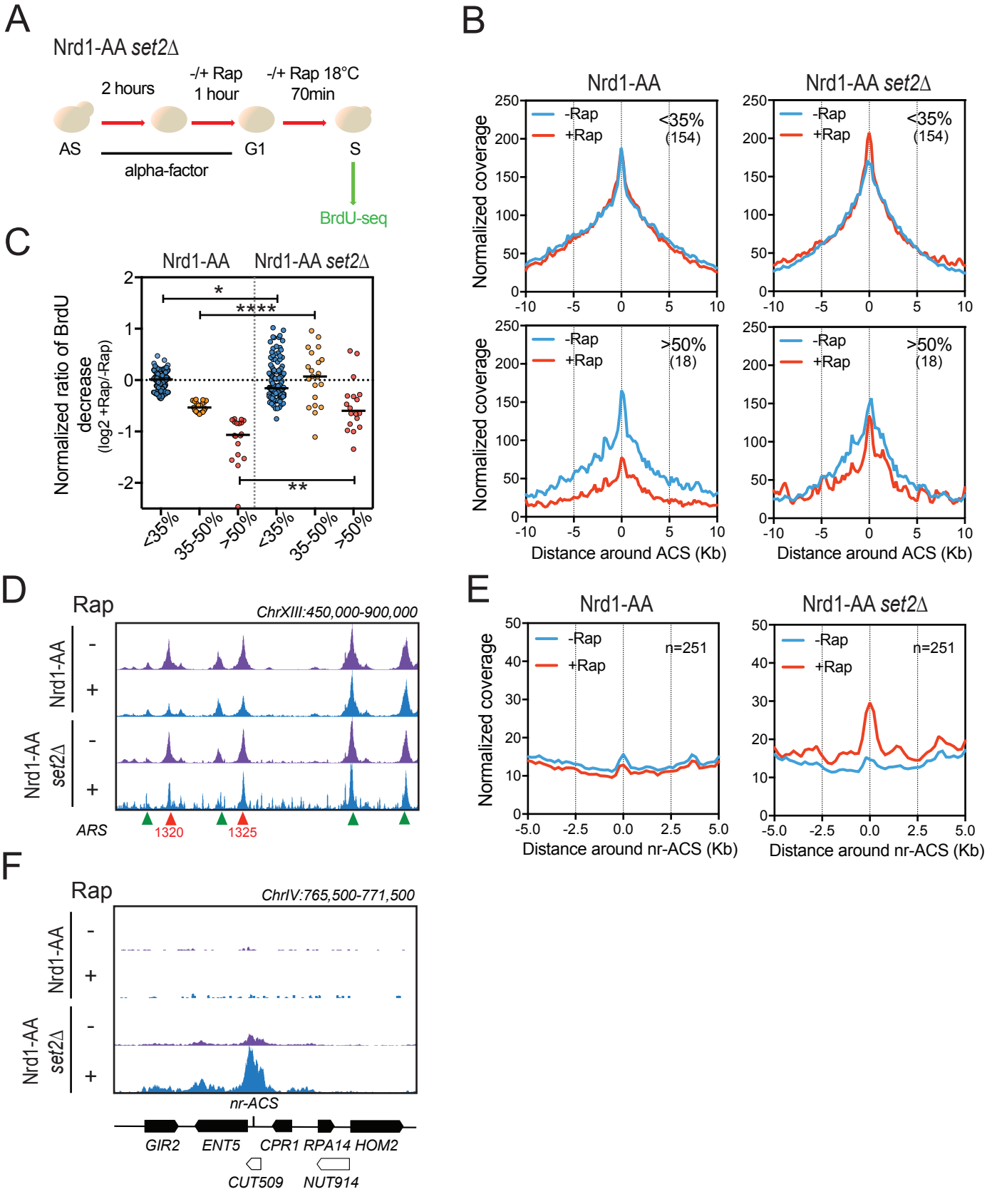

Figure 6

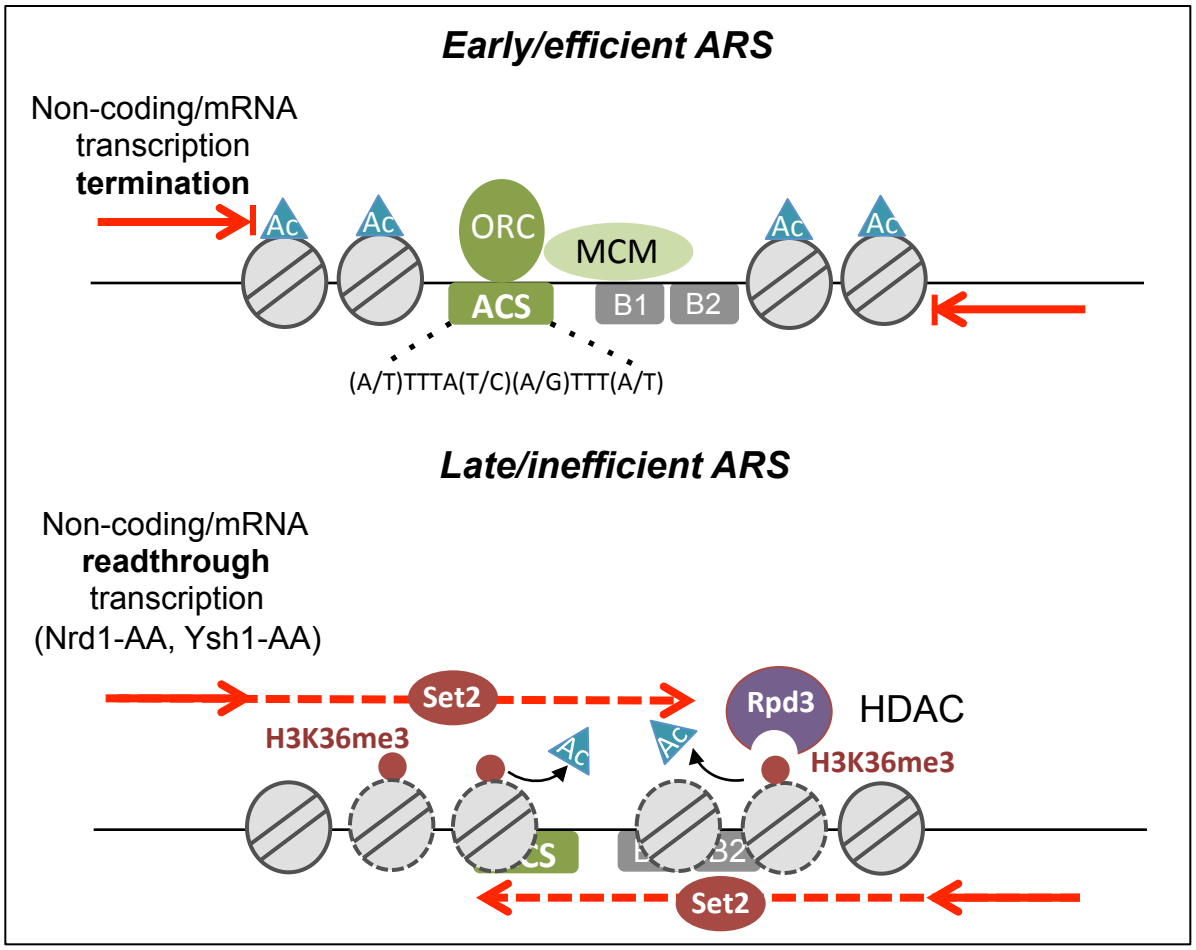
Early/efficient ARS
Non-coding/mRNA transcription termination
Ac
Ac
ORC
MCM
Ac
Ac
ACS
B1
B2
(A/T)TTTA(T/C)(A/G)TTT(A/T)
Late/inefficient ARS
Non-coding/mRNA readthrough transcription (Nrd1-AA, Ysh1-AA)
Set2
Rpd3
HDAC
H3K36me3
Ac
Ac
H3K36me3
Set2

Supp. Figure1

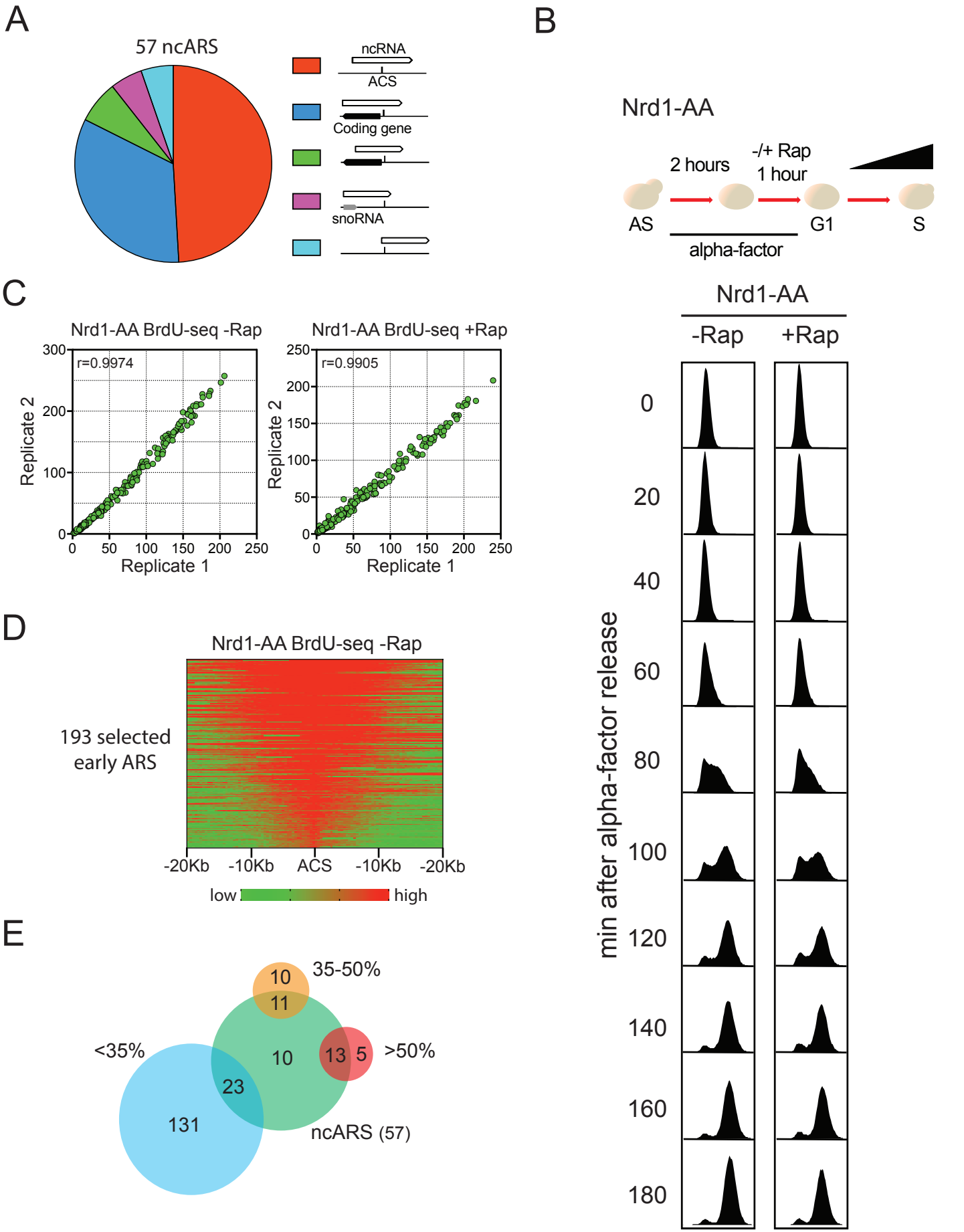

Supp. Figure 2

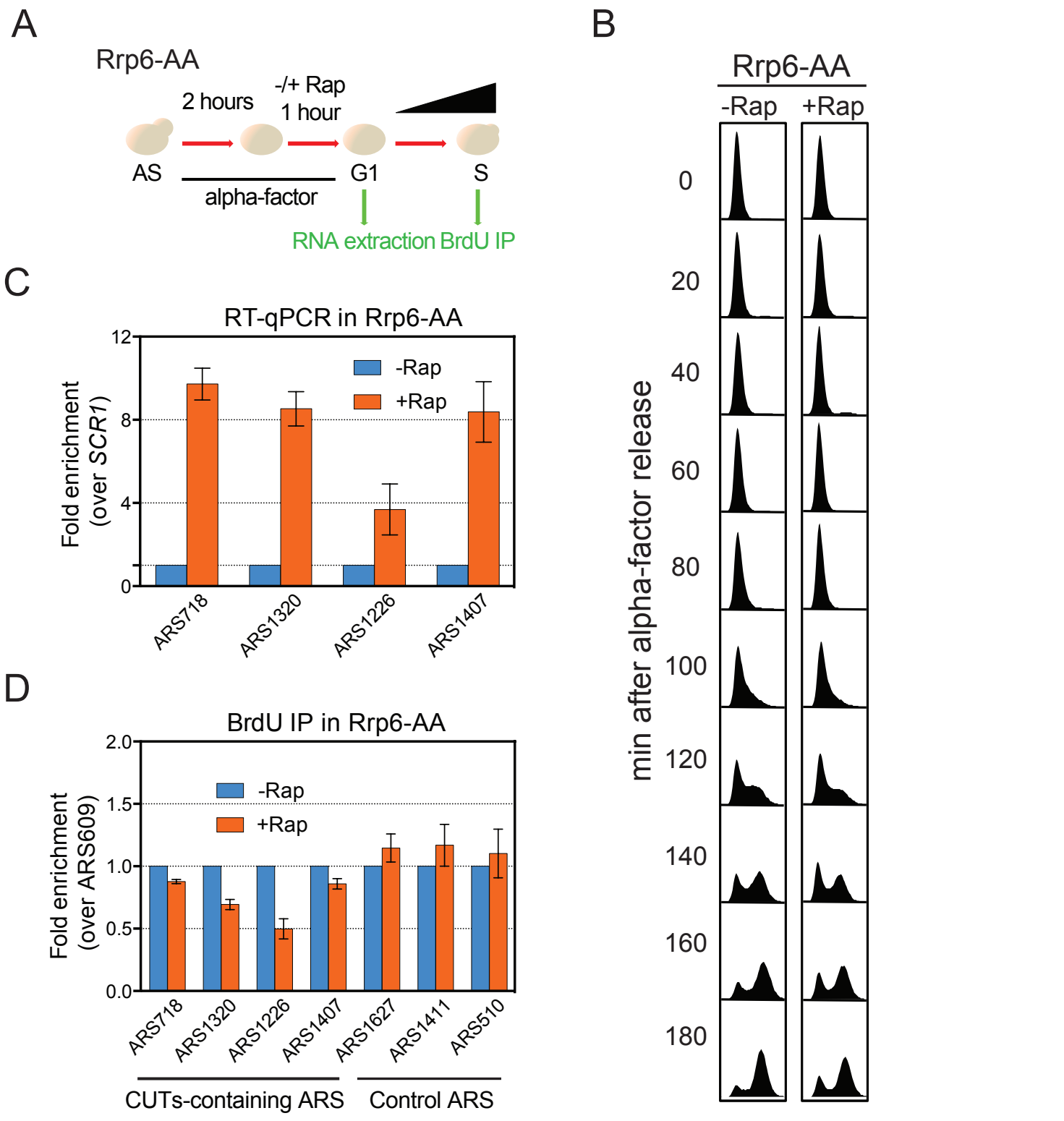

Supp. Figure 3

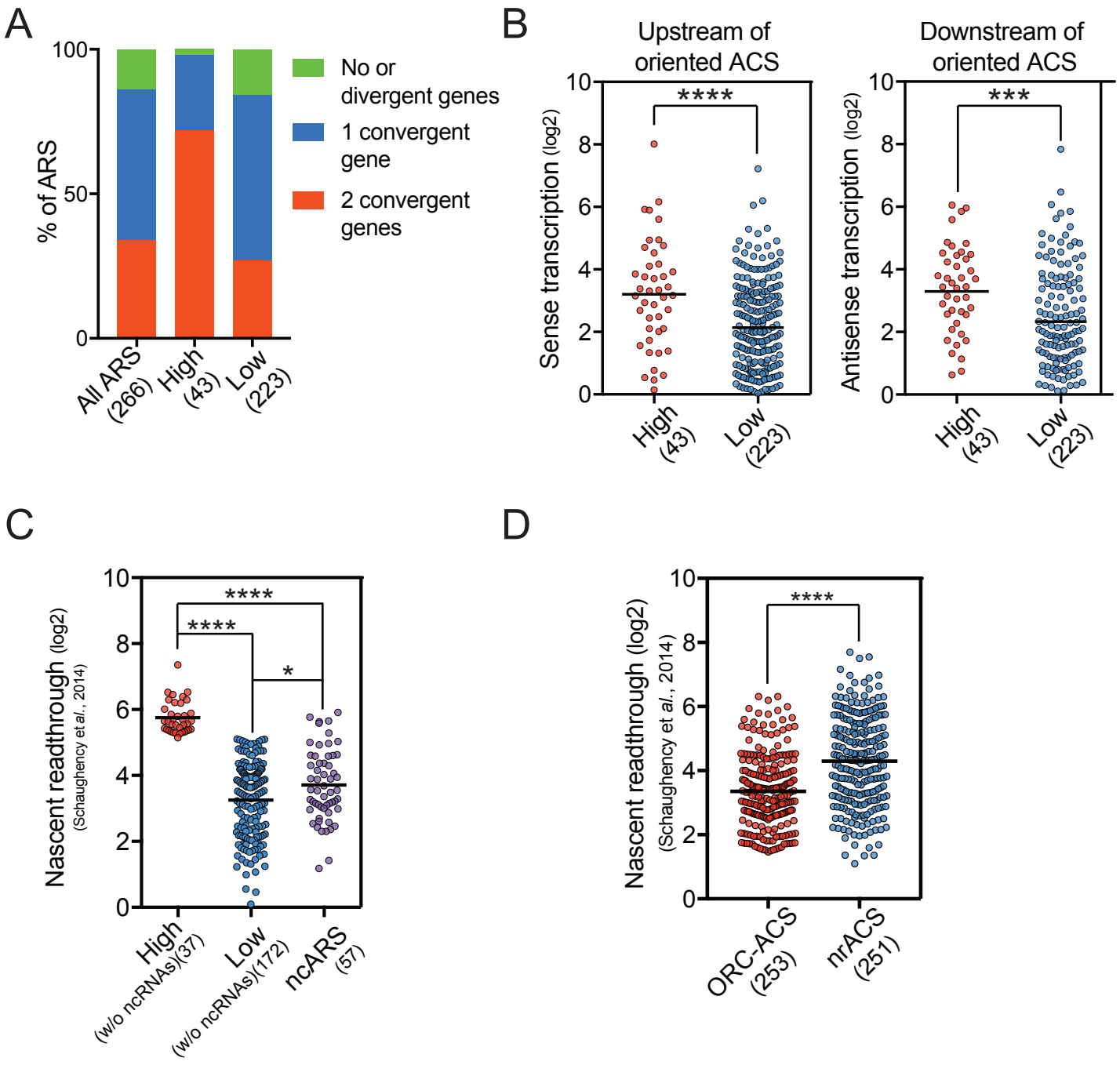

Supp. Figure 4

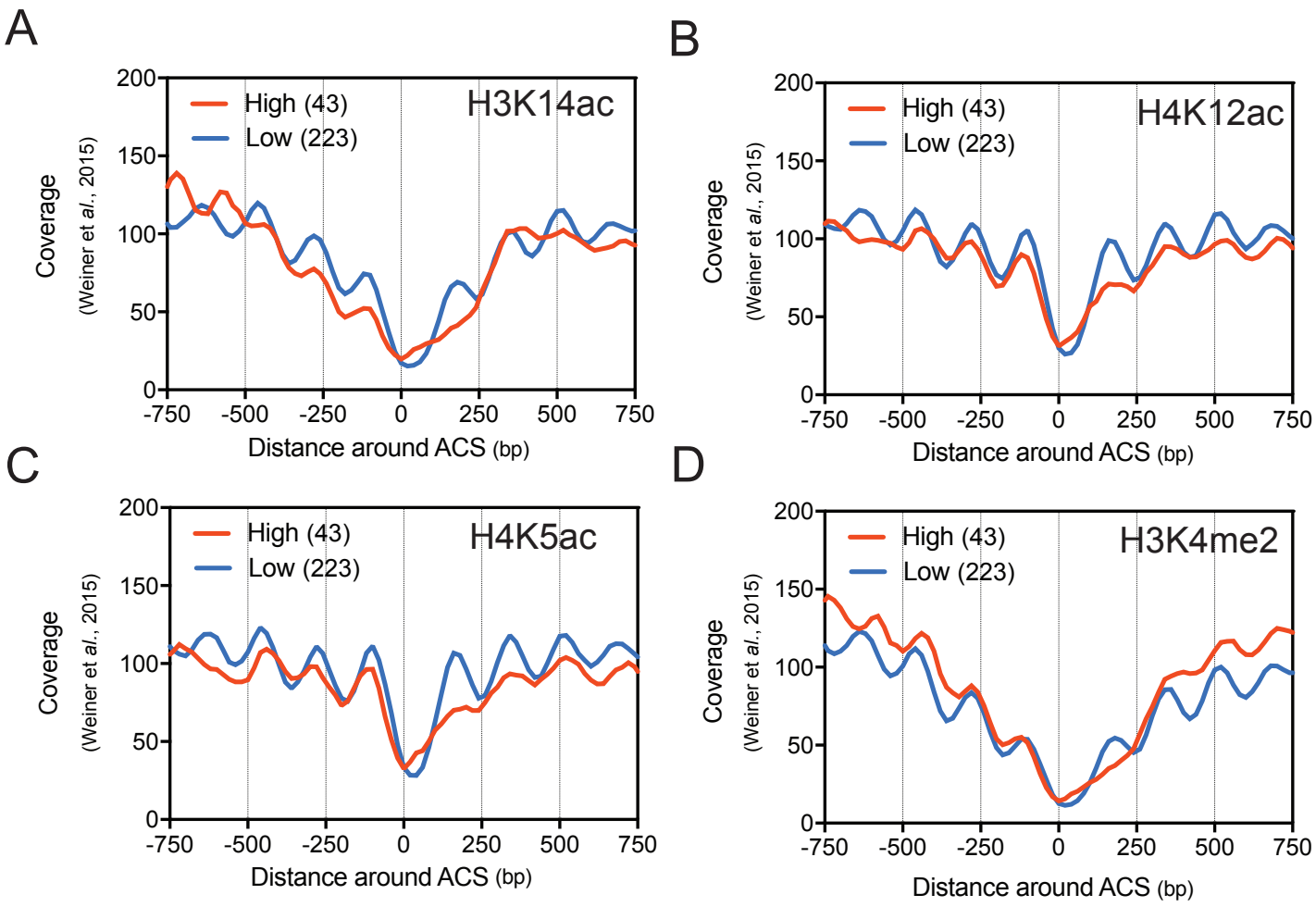

Supp. Figure 5

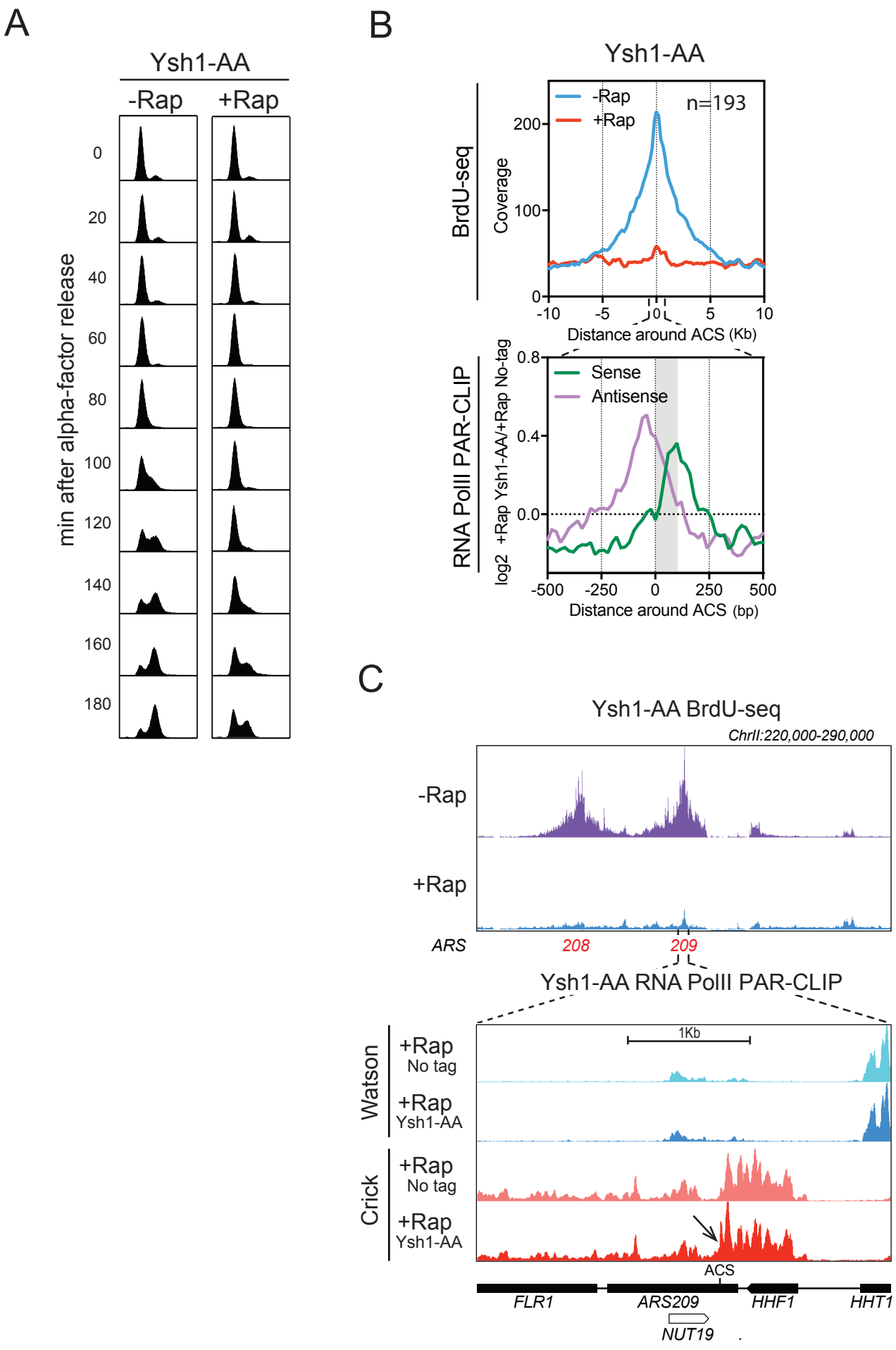

Supp. Figure 6

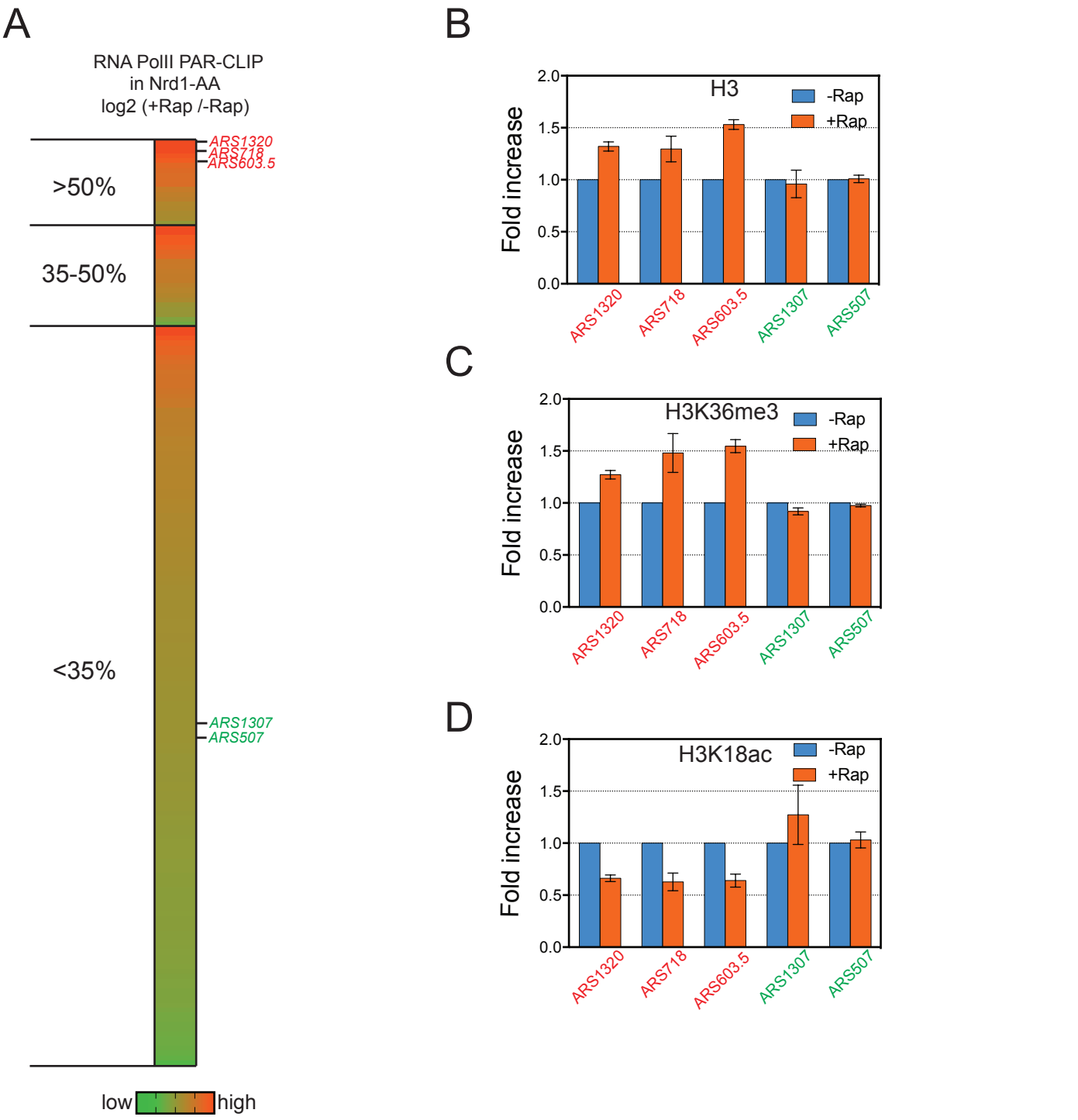

A

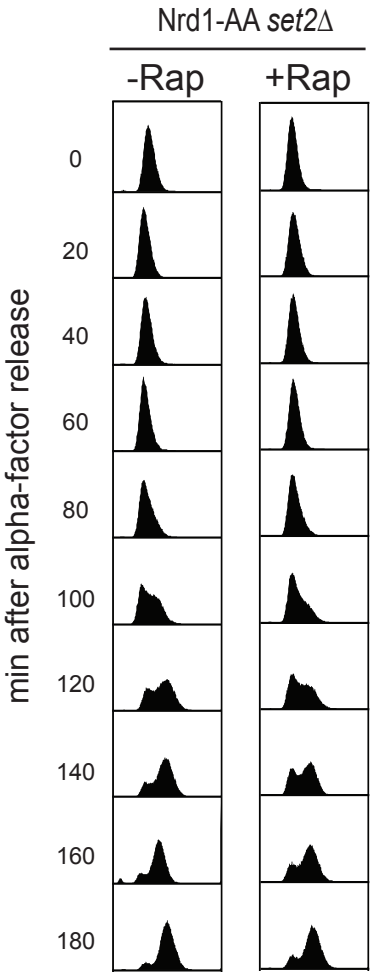
Nrd1-AA set2Δ
-Rap
+Rap
min after alpha-factor release
0
20
40
60
80
100
120
140
160
180

B

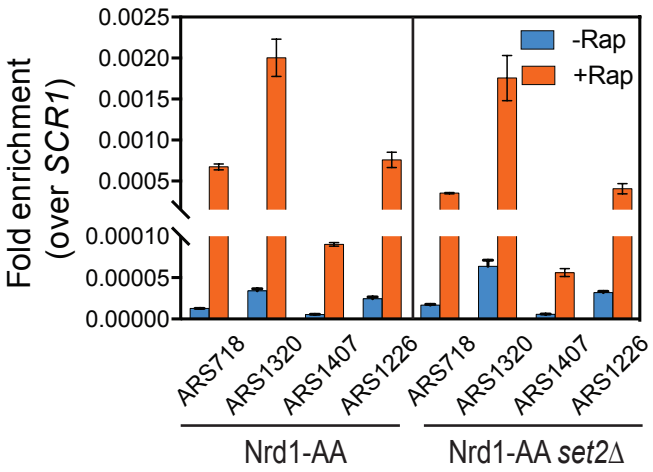
Fold enrichment
(over SCR1)
0.0025
0.0020
0.0015
0.0010
0.0005
0.00010
0.00005
0.00000
-Rap
+Rap
ARS718
ARS1320
ARS1407
ARS1226
ARS718
ARS1320
ARS1407
ARS1226
Nrd1-AA
Nrd1-AA set2Δ